



## Lessons learned in coupling atmospheric models across scales for onshore and offshore wind energy

5 Sue Ellen Haupt<sup>1</sup>, Branko Kosovic<sup>1</sup>, Larry K. Berg<sup>2</sup>, Colleen M. Kaul<sup>2</sup>, Matthew Churchfield<sup>3</sup>,  
Jeffrey Mirocha<sup>4</sup>, Dries Allaerts<sup>5</sup>, Thomas Brummet<sup>1</sup>, Shannon Davis<sup>6</sup>, Amy DeCastro<sup>1</sup>,  
Susan Dettling<sup>1</sup>, Caroline Draxl<sup>3</sup>, David John Gagne<sup>1</sup>, Patrick Hawbecker<sup>1</sup>, Pankaj Jha<sup>4</sup>,  
Timothy Juliano<sup>1</sup>, William Lassman<sup>4</sup>, Eliot Quon<sup>3</sup>, Raj K. Rai<sup>2</sup>, Michael Robinson<sup>6</sup>, William  
10 Shaw<sup>2</sup>, Regis Thedin<sup>3</sup>

<sup>1</sup> National Center for Atmospheric Research, Boulder, CO, 80301, USA.

<sup>2</sup> Pacific Northwest National Laboratory, Richland, WA, 99354, USA.

<sup>3</sup> National Renewable Energy Laboratory, Golden, CO, 80401, USA.

<sup>4</sup> Lawrence Livermore National Laboratory, Livermore, CA, 94550, USA.

15 <sup>5</sup> Delft University of Technology, The Netherlands <sup>6</sup> Wind Energy Technology Office, US Department of Energy, Washington, D.C., 20585, USA.

*Correspondence to:* Sue Ellen Haupt (haupt@ucar.edu)

20

**Abstract.** The Mesoscale to Microscale Coupling team, part of the U.S. Department of Energy Atmosphere to  
electrons (A2e) initiative, has studied various important challenges related to coupling mesoscale models to  
microscale models for the use case of wind energy development and operation. Several coupling methods and  
techniques for generating turbulence at the microscale that is subgrid to the mesoscale have been evaluated for a  
25 variety of cases. Case studies included flat terrain, complex terrain, and offshore environments. Methods were  
developed to bridge the *terra incognita*, that scale from about 100 m through the depth of the boundary layer. The  
team used wind-relevant metrics and archived code, case information, and assessment tools and are making those  
widely available. Lessons learned and discerned best practices are described in the context of the cases studied for  
the purpose of enabling further deployment of wind energy.

30

### 1. Introduction

Whether one is planning for where to deploy future wind farms, micrositing turbines within a wind farm, or  
designing optimal wind farm control, it is crucial to include the impacts of the large-scale (mesoscale, meaning  
35 thousands to hundreds of thousands of meters) flow as well as to model at the microscale (on the order of meters to  
tens of meters). As much of the energy of the atmosphere resides in the largest scales, correctly modeling those  
scales as well as the turbulence and energy dissipation at the microscale provides the most accurate picture of the  
flow and energy available for harvest.



40 The models for the two scales tend to be disparate, however. Although both sets of models are numerical  
discretizations of the Navier Stokes equations, they are built for different purposes. The mesoscale models are  
formulated for weather forecasting, have larger grid spacing over larger domains, and include parameterizations of  
many of the processes that are important for correctly modeling atmospheric flow, such as radiative transfer (short  
45 wave incoming and long wave outgoing), boundary layers, surface layers, cloud microphysics, land surface models,  
and more. Including such parameterizations is necessary to predict the flow accurately. Mesoscale models are also  
initialized with initial and boundary conditions from global models, which include the day-to-day weather  
fluctuations. On the other hand, microscale models are able to resolve details of terrain and wind turbines at a scale  
not available to the mesoscale models. But the microscale models do not include all of the atmospheric physics  
parameterizations of the mesoscale models. Thus, the solution to obtaining accurate flow prediction representing all  
50 relevant scales is to couple the models at these scales.

Such coupling has long been a goal of modelers, but there have been a myriad of issues to work out. For instance,  
the mesoscale models are fully compressible while microscale models are typically incompressible or Boussinesq.  
Treatment of surface conditions is often inherently different. The gap between the typical resolutions of the two  
55 types of models – between about 100 m and traditionally 1000 m – known as the inner “grey zone” or the *terra  
incognita*, has been difficult to bridge (Wyngaard, 2004). One must find ways to initiate turbulence at the microscale  
that is not resolved at the mesoscale. Adding complexity, whether it comes from complex terrain or coupling  
atmosphere to ocean and wave models, complicates the picture and requires separate treatment. Assessing how the  
models perform must be accomplished in the context of wind energy needs. The uncertainty of the model results  
60 should be quantified to be most useful. And finally, how can modern techniques such as improved parameterizations  
and machine learning be leveraged to improve modeling?

As part of the U.S. Department of Energy (DOE) Atmosphere to electrons (A2e) initiative, the Mesoscale to  
Microscale Coupling (MMC) team was charged with studying these issues and more. The goal of the project has  
65 been to improve coupling between mesoscale and microscale simulations via enhanced guidance and new strategies  
for setting up simulations and for the development of new tools that can be used across the community. This  
philosophy recognizes that including the mesoscale forcing is critical to modeling the full energy transfer across  
scales in the atmosphere. Specific objectives include:

- 70 • Apply verification and validation techniques to the new modeling tools and develop estimates of the  
uncertainty,
- Reduce turbulence spin-up time in microscale simulations and hence decrease their computational cost,
- Improve the surface layer treatment in microscale models to more accurately simulate wind speed and shear  
over the rotor diameter,
- Develop best-practice guidance for the community,
- 75 • Prepare and document a suite of software tools that can be used across the community, and
- Transition MMC research to the offshore environment.



Figure 1 illustrates the team’s approach. The goal is to provide more realistic turbulence-resolving simulations through coupling these scales. The team leveraged a case study approach to address these issues (Haupt et al., 2019).

80 By working in the framework of studying particular situations for which we have observations, we can better develop and assess tools to best match real-world situations, which is particularly important for studying nonstationary meteorological conditions (such as frontal passages, thunderstorm outflows, baroclinic systems, and low-level jets) or when considering changes of atmospheric stability associated with the diurnal cycle. In essence, the objective is to have the microscale model “follow” the mesoscale model through dynamic changes while

85 appropriately modeling the fine-scale behavior of the flow. The approach is to select case studies from field programs or observational data to identify challenging atmospheric conditions and test methods to simulate them. Most of these datasets are from DOE-sponsored facilities in flat and complex terrain as well as from offshore sites. The mesoscale modeling has focused on the widely used community model, the Weather Research and Forecasting (WRF) model (Skamarock et al., 2008). Several microscale models have been tested, including the large-eddy simulation (LES) version of WRF (WRF-LES) that can be run online, and several offline models that will be

90 discussed below. Some aspects of the coupling that merit study include the surface and boundary conditions, bridging the *terra incognita*, initializing turbulence at the microscale that is not resolved at the mesoscale, the coupling methods themselves, and dealing with complexity. The testing is grounded in rigorous verification and validation configured specifically for wind energy plus uncertainty quantification, which

95 emphasizes determining parametric uncertainty of turbulence modeling in microscale simulations.

## Mesoscale to Microscale Coupling (MMC) Overview

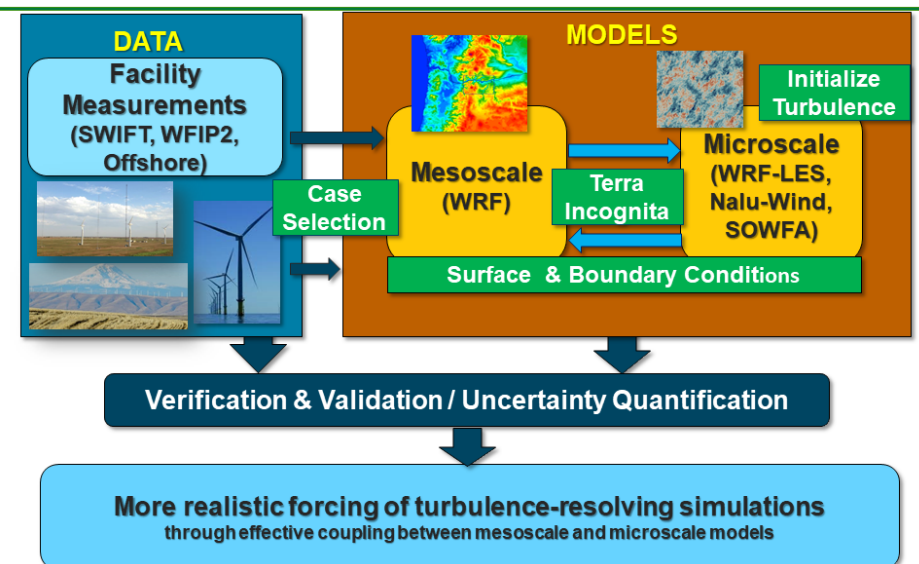


Figure 1: The MMC team’s case-based approach to addressing challenges of coupling the mesoscale to the microscale.



100 An emphasis of the project is testing, evaluating, and comparing multiple methods of coupling the outer mesoscale  
flow to the microscale flow. Some methods use a single model (currently, WRF) at both scales, which ensures  
continuity across scales. Other methods incorporate forcing information from the mesoscale into a stand-alone  
microscale model. This work is based on several preliminary investigations using WRF for both internal (Liu et al.,  
2011; Mirocha et al., 2014b; Muñoz-Esparza et al., 2014; Muñoz-Esparza et al., 2015) and external (Zajackowski  
105 et al., 2011; Gopalan et al., 2014) MMC, showing both promise and direction for future development. Rigorous  
comparisons of methods for different conditions and use cases provide insight into best practices. Another effort  
seeks to compare different methods of generating turbulence in the microscale models that is unresolved by the  
mesoscale forcing. The turbulence generation intercomparison was greatly facilitated by the development of Python-  
based assessment tools that are used via shared Jupyter notebooks. This effort includes design, testing, and  
110 deploying common code bases to simulate and assess the flows, which are now available on the public MMC  
GitHub.

The team has archived simulation codes and model workflows for a range of case studies that can be used as a  
starting point for users to develop their own applications. Model codes, preprocessing, and postprocessing scripts are  
115 available on GitHub at <https://github.com/a2e-mmc>. Online documentation resides in a ReadtheDocs:  
<https://mmc.readthedocs.io/en/latest/>. The archive includes Jupyter notebooks of Python assessment tools to  
compare the model output to observational data using metrics targeted to wind energy applications. The goal of the  
code and workflow release is to promote high-fidelity coupled simulation capability to advance wind energy  
deployment through better knowledge of the atmospheric conditions that drive energy harvest in wind farms.  
120 Modelers are invited to test our models and workflows available at the GitHub site listed above.

This paper describes what we have learned about some of the difficult issues of coupling (Section 2), presents case  
studies that were accomplished (Section 3), and discusses how enhanced methods, such as improved  
parameterizations and machine learning, can help accomplish our goals (Section 4). Section 5 concludes with a  
125 summary and lessons learned plus suggests where future research should focus. Recommendations for best practices  
are sprinkled throughout the paper.

## 2 Some lessons learned

130

The course of the research has investigated the topics laid out in Section 1, and here we summarize the work that has  
led to lessons we have learned.

### 2.1 The *terra incognita*

135



In coupled mesoscale–microscale simulations, including horizontal grid resolutions falling within the *terra incognita* is almost inevitable. The *terra incognita*, coined by Wyngaard (2004), is the range of horizontal grid spacings where turbulence models used in both mesoscale and LES do not work properly. The MMC project investigated the impact of *terra incognita* in coupled simulations (Rai et al., 2017; Rai et al., 2019). Our work suggests that the impact of the

140 *terra incognita* can be minimized using an appropriate choice of horizontal grid spacing, turbulence modeling (dependent on the horizontal grid spacing), and grid refinement ratio applied between the mesoscale to microscale simulations. The most important consideration is that the horizontal grid spacing of the mesoscale simulation should be at least comparable to the boundary-layer depth. Horizontal grid spacing smaller than the boundary-layer depth produces erroneous structures in the simulated flow. Applying a grid refinement ratio (GRR) that allows simulations

145 to jump over the *terra incognita* not only alleviates the problem but also reduces the number of computational domains. A larger value of GRR, however, also increases the fetch needed to generate turbulence on nested domains due to the inertia of larger structures transported from the parent domain. The need for a larger fetch can be mitigated by applying perturbations along the inflow boundaries of the domain (Section 2.4). In some situations, it can be beneficial to use the LES three-dimensional (3D) turbulence model (e.g., Smagorinsky, 1963) in the *terra*

150 *incognita* region, provided that the horizontal grid spacing is closer to 100 m, and then jump to grid spacing larger than the boundary-layer depth using the GRR (Rai et al., 2019). However, the use of a 3D LES closure when the grid spacing is too coarse to resolve any of the motions responsible for momentum transport can result in incorrect stress profiles, leading to significant errors in wind speed within the ABL. The recently developed 3D planetary boundary layer (PBL) Mellor–Yamada scheme (Juliano et al., 2022) fills a critical gap in this regard, providing for a

155 consistent representation of transport at scales finer than traditional mesoscale applications, but at scales too coarse to rely upon a 3D LES turbulence closure (Section 4.1).

## 2.2 Surface layer

160 The surface layer (SL) traditionally represents approximately the lowest 10% of the atmospheric boundary layer (ABL), within which the vertical fluxes of heat, momentum, and other constituents are assumed to approach nearly constant distributions with height above the surface. Parameterization of the exchanges of these quantities between the surface and the atmosphere within atmospheric models relies upon various SL scaling relationships, since the vertical grid spacing in such models is generally too coarse to use a no-slip boundary condition. The particular SL

165 scaling employed, along with characteristics of the model spatial discretization, and the turbulence closure employed to model turbulent exchanges above the surface, all interact to influence the application of the surface boundary condition in atmospheric models, and subsequently impact resulting flow and other SL and ABL characteristics.

The most commonly employed SL scaling relationship used within atmospheric models is the Monin–Obukhov similarity theory (MOST; Monin and Obukhov, 1954). MOST provides relationships to parameterize the fluxes between the surface and atmosphere based on a small number of surface and near-surface atmospheric flow parameters. While MOST is well established, relatively simple, and widely used, it is based on a number of

170



assumptions, including uniform terrain, horizontal homogeneity of both surface and atmospheric variables of interest, steady flow and forcing conditions over time, and the appropriateness of ensemble-mean values of the parameterized fluxes. These assumptions are reasonably well satisfied in most historical numerical weather prediction and mesoscale atmospheric simulations, due in part to the use of coarse grid spacing, which satisfies the appropriateness of ensemble mean representations within each grid cell, while also not resolving sharp transitions in terrain features, horizontal heterogeneities, and meteorological forcing. However, the recent transition toward the use of higher resolution in many mesoscale applications sharpens the representation of some or all of these features, all of which increasingly violate the assumptions upon which MOST is based.

While the use of high horizontal resolution violates the applicability of MOST for one set of reasons, the use of high vertical resolution can create additional problems, especially in settings for which a logarithmic mean profile shape is not expected, such as within forest canopies or over significant surface waves or ocean swell. Moreover, care must be taken not to place the lowest model grid cell too close to the surface.

Microscale atmospheric LES models also routinely apply MOST to formulate the surface stresses at each surface grid cell based on the instantaneous time-varying horizontal velocities above. Even under highly idealized conditions satisfying the assumptions of MOST in the aggregate, such models violate the appropriateness of the ensemble-mean assumption.

Despite the above-mentioned caveats, MOST is still routinely applied in atmospheric simulations at all scales, owing primarily to a dearth of alternatives. To improve its applicability, and the performance of simulating flow within the SL more generally, numerous approaches have been developed, including various damping (Mason and Thomson, 1992) and correction factors (Khani and Porté-Agel, 2017); the use of more advanced turbulence subgrid-scale (SGS) models (Bou-Zeid et al., 2005; Chow et al., 2004); taking care to properly set the computational mesh to have the proper width-to-height ratio (Brasseur and Wei, 2010); and the use of additional near-wall stress parameterizations (Brown et al., 2001) to distribute the surface stresses vertically. The impacts of many of these methods on improving LES performance within the WRF model in wind-energy-relevant applications has been examined in Mirocha et al. (2010), Kirkil et al. (2012), Mirocha et al. (2013), and Mirocha et al. (2014b).

SL modeling has also been extended to applications over forested landscapes for which a logarithmic vertical profile of mean wind speed is not observed (see review by Patton and Finnigan (2012)). These methods are based on the addition of momentum sink terms to the governing horizontal momentum equations to account for the increased drag effects of foliage, with the magnitude of the drag expressed in terms of a leaf area index, which represents the surface area of vegetation as a function of height. Modifications to elements of the SGS model, including eddy viscosity coefficients and SGS turbulence kinetic energy (TKE), may also be included in such formulations.



210 Arthur et al. (2019) implemented the plant canopy model of Shaw and Patton (2003) into the WRF model and  
demonstrated the ability of WRF-LES to recover expected distributions of winds and turbulence quantities in an  
idealized plant canopy. Arthur et al. (2019) additionally combined concepts from the plant canopy approach and the  
near-wall stress models used in various LES SGS formulations (Kirkil et al., 2012) to develop a novel distributed  
drag implementation for the parameterized surface stresses. This model applies the expected surface momentum  
stresses as drag terms in the horizontal momentum equations, distributed vertically over the lowest several model  
215 grid cells. When applied in LES using the MOST surface boundary condition, this approach significantly improves  
agreement between simulated mean wind speed profiles and their expected similarity relationships.

In addition to improving the implementation of MOST within atmospheric solvers, significant progress has also  
been achieved in developing an alternative to MOST using machine learning (ML) to relate surface exchange to  
220 relevant atmospheric and surface parameters obtained from observations. Details of this approach are provided in  
Section 4.2.

### 2.3 Coupling methods

225 Over the course of this project, we have explored different frameworks for coupling mesoscale simulations to  
microscale LES. Coupling approaches can be classified according to the following properties: communication  
directionality (i.e., one-way or two-way coupling), communication strategy (i.e., online through system memory or  
offline through file system), information transferred (i.e., direct quantities such as wind speed, temperature, and  
surface fluxes, or indirect quantities such as tendencies from the mesoscale budget), and the information transfer  
230 location (i.e., inflow/surface planes at the LES boundary, or through the entire flow volume). A comparatively low-  
cost method for coupling mesoscale to microscale is via an offline, periodic LES, which includes internal height-  
time varying source terms that provide mesoscale influence on the microscale. For this approach, mesoscale  
simulation output is saved over a one-dimensional (1D) column at a regular temporal interval (e.g., 10 minutes); this  
information is used with data assimilation techniques to force the periodic simulation toward the desired mesoscale  
235 behavior. One way to achieve this forcing is through what we term “profile assimilation,” in which the microscale  
velocity and potential temperature solutions are plane-averaged at each height at a given time. Those resultant mean  
profiles are compared with the desired mesoscale profiles, and the difference is used to determine the amount of  
forcing required to drive the microscale mean vertical profiles to match those of the mesoscale. One of the key  
lessons learned in this study is that with a strong forcing that enforces the microscale mean vertical profiles to very  
240 closely match those of the mesoscale (what we term “direct profile assimilation”), unrealistic turbulent fields  
sometimes form in the microscale simulation. This may be a natural LES response to mesoscale profiles that are  
superadiabatic over too much of their vertical extent. To deal with this, we developed a method that allows the  
microscale simulation more freedom to depart from the exact mesoscale vertical structure (what we term “indirect  
profile assimilation”), but which will follow all the mesoscale trends in time (Allaerts et al., 2020, 2022).  
245 Alternatively, the mesoscale forcing can be included by imposing time-height varying source terms in the



microscale LES. The forcing accounts for large-scale advection and the driving pressure gradient and is extracted from the mesoscale simulation (Draxl et al., 2021). Any of these methods, though, assume a horizontally homogeneous forcing field and are applicable only to homogeneous cases that are well-represented by periodic boundary conditions. For heterogeneous domains, or simulations that resolve turbines, boundary-coupled simulations are more appropriate. Boundary-coupled simulations can be conducted via online or offline coupling.

For offline coupling, the mesoscale output once again needs to be saved at regular temporal intervals to provide boundary forcing for the LES. However, instead of 1D profiles, two-dimensional (2D) planes must be saved, which increases the I/O and storage requirements considerably. Boundary coupling allows for simulation of a heterogeneous domain for resolving complex terrain, mesoscale flows with significant horizontal gradients, or wind farms.

Online coupled cases downscale from mesoscale through nesting, usually within a single code; this allows for a potentially streamlined workflow, as the downscaling usually involves setting runtime input parameters. Advantages of an online coupled simulation is the ability to use consistent numerics and complete atmospheric physics across spatial scales, and the ability to perform two-way coupling. However, because mesoscale meteorology models are usually not developed with LES applications in mind, this coupling approach requires greater overhead and poorly optimized parallelization of computing resources for the LES domain, imposing severe restrictions on the ability to conduct large numbers of simulations. Offline boundary-coupled simulations are therefore able to achieve higher simulation throughput, which is crucial for parameter selection, sensitivity studies, or wind plant design applications. We conducted a series of case studies directly comparing these approaches: one in a flat, fairly homogeneous onshore environment (section 3.1, Allaerts et al., 2020; Draxl et al., 2021; Allaerts et al., 2022) and one in the offshore environment (section 3.5, Thedin et al., 2022). Further case studies demonstrate the use of these techniques in complex terrain (sections 3.3 and 3.4), resolving the coastal boundary (section 3.6), or in the offshore environment with variable shallow water roughness and sea surface temperature (section 3.6).

#### 2.4 Initializing turbulence

LESs are designed to explicitly resolve the energetically important scales of turbulence and the resulting fluxes and transport those motions generate within the flow. Models using grid spacings that are too coarse to resolve those motions must instead rely on parameterizations (e.g., PBL schemes) to represent those processes. Therefore, when forcing LES with mesoscale atmospheric data at the domain boundaries, either online or offline, a domain fetch is required for the resolved scales of motion to appear within the LES flow field, since those motions are not resolved within the inflow data. A similar issue is encountered when forcing LES with observations, as most observational datasets do not contain sufficient spatiotemporal frequency to specify the turbulence field. In each of these cases, the fetch required for resolved-scale turbulence motions to form and equilibrate to the large-scale forcing within the LES domain can be extensive and represents a significant computational burden. Moreover, the flow field within the





fetch will not well represent either the mean and turbulence fields during the process of turbulence spin-up and equilibration. To ameliorate both the computational overhead and flow inaccuracies within LES forced in this manner, several inflow perturbation methods have been developed and examined within the MMC project. These methods have been shown to successfully promote the formation and equilibration of resolved-scale turbulence within LES driven by mesoscale data and low-frequency observations, leading to substantial reductions of computational expense by permitting the use of smaller LES domains while simultaneously improving the accuracy of the flow field beyond the fetch. The inflow turbulence perturbation approaches that were examined within the project are briefly described below.

#### 2.4.1 Stochastic cell perturbation method

The cell perturbation method (CPM) is based on the application of perturbed values of atmospheric temperature or velocity to “cells” (groups of contiguous model grid points in the horizontal and vertical directions) located just within the lateral edges of an LES domain (Muñoz-Esparza et al., 2014; Muñoz-Esparza et al., 2015; Mazzaro et al., 2019). Optimal choices for the amplitude, size and number of cells imparts variability upon the inflow that rapidly generates resolved-scale turbulence. Since the magnitude of the perturbation applied within each cell is drawn from a random distribution with a mean of zero, the method does not impose spatial correlations or turbulence structure explicitly. Rather, the mixture of random amplitudes and spatial correlations among the cells leads to the development of turbulence that is consistent with the large-scale forcing, defined by the ABL depth, surface roughness and temperature fluxes, and the distributions of mean winds and temperature – the latter contained within the inflow.

The CPM has been successfully applied in both idealized and real-data simulations for wind energy applications, including a diurnal cycle over an area of wind energy development in the U.S. Midwest region (Muñoz-Esparza and Kosovic, 2018), during a ramp event interacting with a parameterized wind farm in the Central Great Plains (Arthur et al., 2019), and in offshore resource characterizations in the North Sea (Thedin, et al. 2022) and U.S. East Coast regions (Hawbecker, et al., 2022), in each case showing improvement of the LES wind field, relative to unperturbed simulations

#### 2.4.2 Synthetic turbulence method

Synthetic turbulence, such as the Mann method (Mann, 1998), are applied along the inflow boundaries of the LES domain to help generate realistic turbulence. The Mann synthetic method produces the turbulent winds in the three-dimensional volume, which is converted to a time series of inflow planes employing the frozen turbulence hypothesis. This method uses the spectral tensor of wave vectors to generate the isotropic turbulence and makes it anisotropic by applying the rapid distortion theory to the turbulent wind field. The inputs for controlling the variances of the turbulent field are the length scale and scaling intensity factor that controls the turbulent energy in



320 the flow. If observations are available, we usually adjust the turbulence intensity by scaling the square root of the  
variances from the observations before applying it to the microscale model within the boundary-layer depth.  
Similarly, the frequencies of the turbulent inflow field at the domain boundaries can be adjusted based on the inflow  
wind speed. In addition to the Mann method, synthetic turbulence methods, such as TurbSim (Jonkman, 2006 ;  
Rinker, 2018), can also generate turbulence along the inflow boundaries. Unlike the Mann method, TurbSim  
325 generates inflow planes in the time domain. If observations are available, the simulated turbulence can be forced to  
match an input time series and the structure of the turbulence can be controlled through empirical coherence  
functions. These methods have been compared to CPM for flat terrain (Haupt, et al. 2019,2020) as well as for  
offshore (see section 3.5).

### 330 **2.5 Quantifying uncertainty**

Modeling the atmosphere, at both meso- and microscales, is subject to uncertainty from a variety of sources.  
Uncertainty propagates from the data used to specify initial and boundary conditions (e.g., reanalysis-based flow  
fields, land surface properties, sea surface temperature data), from the form of model closures, and from specific  
335 parameter values used within a closure. Sensitivities to these uncertain factors may display complex, nonlinear  
interactions. Therefore, constraining the impacts on model predictions – particularly when considering mesoscale–  
microscale coupled modeling – is difficult. A powerful, albeit computationally intensive, approach to evaluating  
uncertainty in atmospheric model closures is to generate an ensemble of simulations that sample across a range of  
parameter values. To adequately capture potential nonlinearities in the atmospheric model response, several dozen  
340 or more ensemble members are typically required. However, once such a perturbed parameter ensemble is  
generated, it may be extensively interrogated using a variety of meta-modeling techniques.

In the context of wind energy applications, quantities of interest such as hub-height wind speeds, turbulence levels,  
shear, and veer are known to generally show sensitivity to parameterizations of boundary layer turbulence and  
345 surface fluxes, and these kinds of parameterizations have been most extensively targeted for uncertainty  
quantification under the MMC project and related A2e projects. For example, uncertainty in mesoscale model  
predictions over complex terrain owing to parameter values of PBL and surface schemes was examined by Yang et  
al. (2017, 2019) and Berg et al. (2019). Reassuringly, these studies found that only a few parameters accounted for  
most of the model uncertainty, although the identity of these parameters could vary diurnally and seasonally based  
350 on the dominant state of atmospheric stability. Uncertainty owing to LES subgrid-scale turbulence closure  
parameters in realistic mesoscale–microscale coupled simulations was examined by Kaul et al. (2022) and found to  
trace predominantly to a single parameter (an eddy viscosity coefficient). However, the sensitivity of the modeled  
flow to variations in this parameter was noted to vary significantly between two case studies with nominally similar  
large-scale flow conditions but different smaller-scale flow structures (convective cells versus rolls).

355



Looking forward, much work remains to better characterize uncertainties within both mesoscale and microscale model predictions across a wider range of flow conditions, especially offshore. However, these initial studies give promising indications that uncertainty can typically be traced to a small number of model parameters and that the importance of these specific parameters can be interpreted in terms of flow physics considerations. Furthermore, application of meta-modeling techniques and leveraging machine learning approaches can greatly aid in detecting relationships and patterns within atmospheric model responses. Thus, efforts at uncertainty quantification not only meet a practical need to bound variability in atmospheric model predictions, but also can provide deeper insights to modelers that may ultimately drive improvements in parameterizations.

## 365 **2.6 Challenges of complexity and ways to approach**

Complexity comes into play in many manners for atmospheric flow. For the purposes of enhanced MMC for wind energy applications, we have focused on issues relating to complex terrain and offshore environments, including issues of correctly modeling atmospheric gravity waves but avoiding generating spurious ones.

### 370 **2.6.1 Complex terrain**

The coupling of mesoscale to microscale models using an offline approach (see Section 2.3) allows for the use of a stand-alone microscale LES solver, which brings the ability to use high-quality (in terms of mesh orthogonality) terrain conforming meshes. In complex terrain simulations, the assumption of horizontal homogeneity (often assumed in microscale simulations of the boundary layer) is no longer valid. Adding complex terrain to the simulation implies that periodic boundary conditions are not appropriate, and thus mesoscale coupling must be performed at the boundaries by means of spatiotemporal varying boundary conditions. A few additional complexities arise when performing this coupling.

380 To initialize the flow field in the microscale, the mesoscale solution is mapped onto the microscale domain. However, this mesoscale solution is obtained at a significantly coarser resolutions. In order to avoid unnecessary computational expense, a coarse grid must first be created to allow the mapping. After the mapping, further grid refinement should be performed to bring the domain to the desired microscale resolution. An additional terrain-conforming step must be taken to ensure the high-resolution LES grid is properly conformed to the underlying terrain elevation map. The boundary conditions that come from the mesoscale models only contain mean quantities, and thus the LES-resolved turbulence must be initiated in some way. Due to the inflow–outflow boundary conditions, two main strategies are used: the application of the cell perturbation method (see Section 2.4.1), or to allow the terrain itself to trigger the turbulence. We found that a perturbation technique is recommended because the terrain is only effective at generating the turbulence if it is sufficiently complex, in addition to significant fetch requirements (Hawbecker and Churchfield, 2021). An additional complication can be present in the mesoscale boundary condition, where a single microscale boundary may experience inwards and outwards fluxes, and one must



395 make an appropriate choice of the boundary conditions for both the velocity and pressure, depending on the LES  
code of choice. Finally, the terrain can trigger atmospheric gravity waves under certain stability conditions. The real  
atmosphere extends for tens of kilometers vertically and infinitely horizontally, but a simulation domain is finite.  
Atmospheric gravity waves reflect off of these domain boundaries and constructively or destructively interact,  
creating spurious behavior. Approaches used to mitigate these spurious reflections and interactions are detailed in  
Section 2.6.2.

400 We note that while the stand-alone microscale solver adds complexity to the setup, it allows for greater flexibility.  
Most importantly, it allows for the study of the interaction of realistic weather conditions, complex terrain, and  
turbines. The turbines can be coupled with aero-servo-elastic models using OpenFAST (2022 – see section 3.5.2)).  
In the workflows presented in this paper, the turbine can be represented by actuator disk or actuator line models.  
Note that the stand-alone, offline approach even allows the use of blade-resolved approaches.

405

### **2.6.2 Atmospheric gravity waves**

As discussed in section 2.6.1, complex terrain can trigger atmospheric gravity waves, which microscale simulations  
that include buoyancy effects will capture. In addition to complex terrain, atmospheric gravity waves can be  
410 triggered by certain mesoscale weather patterns, land–sea interfaces, or wind farms themselves. The flow induced by  
these atmospheric gravity waves can be of significant importance, or sometimes it may be of secondary importance.  
But if these waves, whether significant or not to the simulated problem, are allowed to reflect off of domain  
boundaries unchecked, they can cause spurious wave interactions with unreasonable wave amplifications that  
completely pollute the rest of the flow. Our approach of choice to mitigate spurious reflections is Rayleigh damping.  
415 Rayleigh damping is a simple but flexible concept. A layer of some thickness is placed adjacent to a domain  
boundary in which a source term is introduced in the momentum equation that forces the velocity toward a reference  
velocity with some time scale. Often we choose to damp only the vertical velocity component to a zero reference  
state. However, Rayleigh damping is completely general in that the reference velocity can be as complex as a 3D,  
time-varying field. Challenges with Rayleigh damping include choosing an adequate thickness and proper time scale  
420 to effectively damp atmospheric gravity waves. Too weak a damping layer will not completely damp reflected  
waves, but waves will reflect off too strong a layer. An additional challenge arises if the inflow boundary needs to  
be damped, which we find to be the case in all inflow–outflow simulations, because upstream propagating  
atmospheric gravity waves must be damped, but one does not want to damp incoming turbulence.

### **425 2.6.3 The complexity of modeling offshore wind**

When switching from simulating complex terrain on shore to the offshore environment, our initial assumption was  
that the problem became simpler. The offshore environment, due to a “flat” sea surface, seemed ideal for periodic  
idealized simulations. Additionally, there are no heterogeneous surfaces to consider such as trees and cities, but only



430 water. This seemingly simpler problem turns out to be very complex and with fewer observational datasets to  
compare against, it is very difficult to verify simulation accuracy. First, the ocean surface is generally covered in  
waves of varying sizes, traveling in different directions, and with different periods. These waves have a complex  
relationship with the atmosphere and ocean depth (see, for example, Jiménez and Dudhia (2018)) that needs to be  
carefully considered in order to accurately simulate wind speeds within the boundary layer. Secondly, sea surface  
435 temperature (SST) and SST gradients play an important role in determining the stability of the atmosphere above.  
When considering SST gradients in simulations, we are often unable to utilize periodic boundary conditions as  
initially thought. Additionally, while many satellite-derived SST products exist and are used as the lower boundary  
condition for temperature in a model, they are commonly only available once per day and rely heavily on gap-filling  
techniques to produce estimates of SST where clouds have blocked their measurement, leading to biases in SST  
440 datasets (Zuidema et al., 2016). These impacts may be more significant in the near-shore environment in which  
offshore wind is focussed due to the occurrence of coastal upwelling, seasonal and climatological changes in ocean  
currents such as the Gulf Stream, and the propensity for cloud coverage. Finally, there are also characteristics of the  
offshore environment that are infrequently observed over land. Offshore low-level jets in the New York Bight –  
where offshore wind plants are being developed – have been frequently observed to have jet noses below 100 m.  
445 This means that the shear across the rotor will be extremely complex, as hub height for offshore turbines will be  
above the jet nose. Another example is the propensity of extreme weather events in the offshore and coastal  
environments. Hurricanes and other tropical disturbances commonly weaken as they move on shore due to increased  
friction, or over colder seas, which reduces the latent energy that powers them. Such storms can remain quite strong  
while located over warm ocean waters; however, the rate of storm motion can also play a role, as slower storm  
450 movement can mix cooler water from below the thermocline up toward the surface, reducing the energy supply.  
Upper level wind shear can also reduce the organization of the storm, leading to weakening or dissolution. All of  
this leads to a very complex modeling framework requiring the coupling of ocean and atmospheric models (Shaw et  
al., 2021).

## 455 **2.7 Wind energy relevant assessment and code availability**

To enable accurate assessment and repeatability of our science results, we have made all the essential components of  
our studies publicly available. These components include (1) the problem definition, including data exploration,  
curation, and transformation into useful simulation inputs; (2) the actual simulation inputs, including model  
460 configuration files and scripts; and (3) postprocessing and synthesis of output. For this purpose, we have established  
the A2e-MMC GitHub organization for archiving and disseminating our work (<https://github.com/a2e-mmc>). This  
public GitHub organization hosts Python analysis code, Python analysis notebooks, code-specific input files, as well  
as our MMC-specific version of the WRF model that tracks the community version (currently v.4.3), each  
constituting a separate version-controlled repository. For every study in this project, the team has adopted workflows  
465 based on a common set of analysis and simulation codes within this framework, thus ensuring apples-to-apples  
comparisons between results. To complement the technical content on GitHub, we have also created a ReadTheDocs



documentation site to provide an easily accessible high-level overview of our project's accomplishments, describe our capabilities, and link to the resources on GitHub wherever appropriate (<https://mmc.readthedocs.io/en/latest/>). We believe that in combination the GitHub and ReadTheDocs will serve as a living record of the MMC project, as well as provide flexible and adaptable documentation for future related projects.

### 3 The value of case studies

The team has developed and archived simulation codes and model workflows for a range of case studies that can be used as a starting point for users to develop their own applications. The value of using a case study approach includes the ability to choose real-world phenomena to model where observational data exist to validate our models. That allows us to test different modeling approaches and techniques to discern which are most appropriate for the particular situation. The cases that are curated are described briefly in the following sections, along with some lessons learned for each.

#### 3.1 Flat terrain diurnal cycle

To develop and test methods for coupling so that the microscale follows changes at the mesoscale, an early case study of a diurnal cycle in flat conditions was chosen. This nonstationary case includes time-varying hub height wind speed and direction, shear and veer, and turbulence intensity. For such a case, accurate downscaling of energy from the mesoscale is important for predicting realistic turbulent flow feature in the wind farm operating environment.

Surrounded by grassland with no significant terrain changes within hundreds of miles, the Scaled Wind Farm Technology (SWiFT) facility located in the southern Great Plains in West Texas forms an ideal flat terrain test site. There are several meteorological measurement facilities near the SWiFT site hosted by Texas Tech University's National Wind Institute (Hirth and Schroeder, 2014), including a tall meteorological tower and a radar wind profiler with radio acoustic sounding system. In addition to the ideal terrain and availability of observational data, the site is also chosen for its relevance to onshore wind energy installations in the United States. Details of the atmospheric characterization are provided in Kelley and Ennis (2016).

From available data, the evening transition from 8 to 9 November 2013 was identified as a synoptically quiescent diurnal cycle leading to nonstationary flow conditions at heights relevant to wind energy. The evolution of flow parameters including wind speed, turbulence intensity, and virtual potential temperature follows a typical diurnal pattern, featuring a morning transition, daytime convective boundary layer, afternoon/evening transition, and a nocturnal low-level jet. The relatively simple geographical and meteorological conditions of the SWiFT diurnal cycle make it an ideal case to study the performance of internal coupling methods throughout various atmospheric stability regimes. The case has been used to evaluate existing coupling methodologies (Draxl et al., 2021) as well as



505 to develop new techniques (Allaerts et al., 2020, 2022). More information about the modeling setup, data sources,  
and assessment codes may be found at: <https://mmc.readthedocs.io/en/latest/cases/swift.html>.

510 Among the various lessons learned from this flat terrain diurnal cycle case, perhaps the most important one was  
regarding the division of responsibilities between the mesoscale and the microscale solvers in an MMC framework.  
The trends in the mean flow are set at the mesoscale level, and the microscale solver cannot correct for large biases  
515 in mean-flow quantities or erroneous timing of large-scale events like the evening transition. The task of the  
microscale solver is to fill in information on the unsteady, three-dimensional turbulent structures, which was often  
accompanied by an improvement in the prediction of wind shear and mean turbulence statistics inside the boundary  
layer, even in the relatively simple conditions of the SWiFT diurnal cycle. Further, the SWiFT case also highlighted  
the need for more high-quality data extending up to higher altitudes for validation purposes. Despite the available  
520 meteorological tower being taller than typically deployed towers, many boundary-layer processes with relevance to  
wind energy take place above 200 m. For example, the low-level jet that developed during the SWiFT diurnal cycle  
was predicted to attain its maximum wind speeds at a height between 250 and 350 m, but there was insufficient data  
to validate this finding. Moreover, meteorological towers only present observations from a single column, which  
means they cannot be used to assess how well the spatial variations in the turbulent flow fields are predicted.

520

### 3.2 Frontal passage causing a wind ramp

A second case study (Arthur et al., 2020) leveraged MMC techniques to conduct simulations of a wind farm during a  
frontal passage, for which rapid changes in wind speed, direction and temperature, and atmospheric turbulence were  
525 observed. One of the key benefits of mesoscale–microscale coupling is the ability to examine wind energy  
phenomena at the wind plant scale while resolving time-varying forcing from the mesoscale. The simulations  
demonstrated the ability to capture the relevant mesoscale meteorological phenomena on a typical mesoscale  
simulation domain, downscale those features to an LES domain containing a section of an operating wind plant,  
represented as generalized actuator disks (GADs; Mirocha et al., 2014a), and simulate the interactions between the  
530 time-varying meteorological flow and turbines, including wakes, power extracted, and turbulence phenomena. This  
case study demonstrates the viability of fully online-coupled MMC simulations in WRF to address important issues  
in wind plant behavior under realistic atmospheric operating conditions.

### 3.3 Complex terrain case with high wind speeds and convective conditions

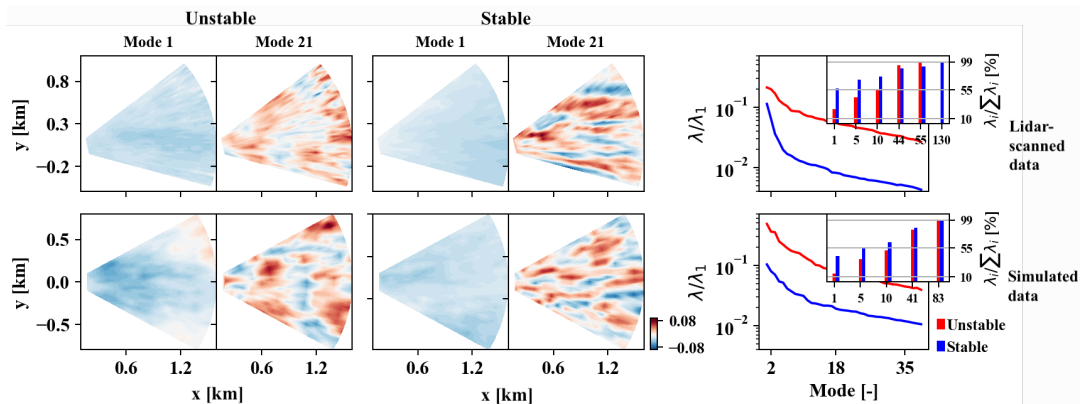
535

The purpose of this complex terrain case study is to examine the flow structures near the surface, which depend on  
many factors, including surface forcing. We investigated coherent structures present in the flow measured using  
scanning lidar deployed near Wasco, Oregon, during the WFIP2 campaign (Wilczak et al., 2019) and those  
simulated using WRF LES. The simulations utilized WRF to WRF-LES for the unstable condition case on 21  
540 August and stable conditions on 14 August 2016 for the westerly flow. The model output was sampled in a way



consistent with scanning lidar data using plan position indicator scanning. For both stability conditions, 90 east sectors, each 1 minute apart, were selected from the simulations and used to compute the spatial proper orthogonal decomposition (POD) modes and energy (Berkooz et al., 1993). The actual lidar data of the unstable case uses 49 east sectors with wind speed and heat flux values similar to those in the simulations, 5–7 m/s and ~350 W/m<sup>2</sup>, respectively. For the stable case, the actual lidar data employs 160 east sectors with a wind speed of 10–12 m/s and heat flux ~-30W/m<sup>2</sup>, similar to the simulated values. Figure 2 shows the spatial POD modes 1 and 21 and the POD energy distributed among many modes for the simulated and actual lidar data for the two stability conditions. The first POD mode in all cases shows the most significant coherent structures, followed by smaller structures for the increasing mode number. For the given stability conditions, the simulated and lidar cases showed similar shape and size variations for all modes. The first few modes (modes < 5) show similar spatial structures in the POD modes for all stability conditions. However, they exhibit different spatial structures for the higher POD modes. For instance, mode 21 in the unstable case shows large open-cell-like structures, whereas mode 21 in the stable case shows streak-like structures oriented in the predominant wind direction. This variation of flow structures in different modes can be attributed to the forcing function. POD energy shown in Fig. 2 (right panels) depicts the turbulent energy associated with each coherent structure starting from mode 2. The unstable conditions consistently exceed the POD energy (for mode >1) in both simulated and observed lidar data. The cumulative energy (Fig. 2, inset) indicates that the first mode of the stable condition case contains larger POD energy than the unstable condition case and requires larger modes to represent the energy in the flow in observational data. Although the trend of varying POD energy shows similarities between the two cases, their magnitude and the energy spread among the modes differ. Overall, the POD modes of the different stability cases demonstrate that the simulations capture the important features of coherent structures present in actual lidar data.

Figure 2: Spatial POD modes 1 and 21 for the unstable (first and second columns) and stable (third and fourth columns) condition cases, and POD energy among the first several modes (fifth column) and their cumulative energy (in the inset). Panels in the top and bottom rows represent the results from observed and the simulated data.







### 570 **3.4 Complex terrain case using 3D PBL**

This second complex terrain case also leverages measurements made during the WFIP 2 campaign, which covered many stability conditions, including cold air pools (CAPs) that tend to develop during synoptically quiescent periods. To study the ability of the 3D PBL scheme to capture such features, we chose a case from 10–20 January  
575 2017 when a robust CAP was observed in the Columbia River Gorge. Such events are often challenging to represent accurately in mesoscale simulations due to the relatively small-scale boundary layer processes that must be parameterized. To better understand the spatial variability in meteorological and turbulence characteristics during the CAP lifecycle, we conducted WRF simulations following the High-Resolution Rapid Refresh (HRRR) reforecast configurations that were run for the WFIP2 project. For these simulations, the Mellor–Yamada–Nakanishi–Niino  
580 (MYNN; Nakanishi and Niino, 2006) scheme is run in the inner domain (horizontal grid cell spacing,  $\Delta = 750$  m) of a nested two-domain setup. A novelty of this study is the use of NCAR’s 3D PBL parameterization (Kosovic et al., 2020; Juliano et al., 2022; Eghdami et al., 2022; Rybchuk et al., 2022), which was implemented into the WRF model for high-resolution mesoscale simulations. More information about the modeling setup and codes may be found at:  
<https://mmc.readthedocs.io/en/latest/cases/wfip2.html>.

585 Several key findings emerged from the WFIP2 CAP study, with additional details reported by Arthur et al. (2022). First, turbulence kinetic energy (TKE) measurements from the profiling lidar at the Gordon’s Ridge site reveal that, compared to MYNN, the 3D PBL simulation more accurately represents the vertical and temporal variability in TKE. As a result, wind speed errors were lower in the 3D PBL simulation, especially during the CAP erosion  
590 period, which has been especially difficult to model (Adler et al., 2021). To better understand the leading cause of the improved performance by the 3D PBL compared with MYNN, we performed a sensitivity analysis using the 3D PBL scheme framework. More specifically, we modified the turbulence closure approach as well as the turbulent length scale/closure constants formulation. The main reason for the improvement in TKE prediction is primarily related to the different turbulent length scale/closure constants formulation. For 3D PBL simulations under  
595 convective conditions, Juliano et al. (2022) reported similar findings regarding the primary importance of turbulent length scale/closure constants formulation.

### **3.5 Offshore wind case with a long offshore fetch**

600 The MMC techniques developed for onshore studies were tested for a first offshore scenario at the FINO1 research tower, located in the North Sea. This case is representative of low roughness and low turbulence and leverages measurements from the FINO towers and data from the Alpha Ventus wind energy plant.

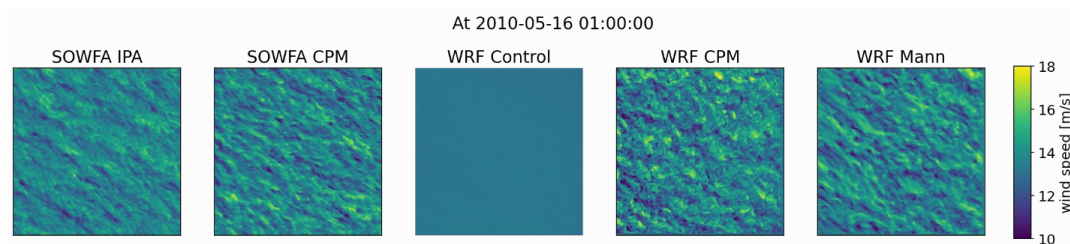
#### **3.5.1 Comparison of coupling methods and turbulence generation methods**



605 Comparisons are made between members of an ensemble of mesoscale simulations, different coupling methods with several models, and different turbulence generation schemes. The goal of the comparison is to assess the performance of each approach and highlight their strengths and weaknesses. The approaches compared include:

- WRF to SOWFA using the indirect profile assimilation technique (IPA),
- WRF to SOWFA using the CPM at the inflow boundaries,
- 610 • WRF to WRF-LES without any added turbulence generation (control simulation),
- WRF to WRF-LES using the CPM at the inflow boundaries, and
- WRF to WRF-LES using the Mann model to generate the large-scale turbulence.

The domains used were 6 x 6 km, with the exception of SOWFA IPA, which had a 3 x 3 km extent. The larger  
615 extent allowed a fetch for turbulence development. The results shown here represent the developed-flow region, near the outlet boundaries. A qualitative visualization of the resulting flowfield is given in Fig. 3.



620 **Figure 3: Wind speed at 0100 local time on 16 May 2010 around the FINO1 location for the different methods investigated. The original domains contains fetch region, showing only a developed-turbulence 3 x 3 km subdomain.**

Comparisons across the methods and observation data were made in terms of vertical profiles, power spectral density content, correlations, and integral scales. WRF Mann and both CPM methods overestimated the energy content, with the SOWFA IPA matching well the content with respect to observations up to frequency related to the LES cutoff. The WRF control case showed very little content, as expected. The SOWFA IPA case is the only one  
625 where the turbulence was not triggered by a numerical method, but rather developed using doubly periodic boundary conditions. All of the vertical profiles are comparable, with the exception of the control simulation, which due to the lack of resolved turbulence exhibited a larger shear profile. Correlation maps were calculated for every point in the domain with respect to the central point, and correlation curves were obtained in the along-wind and cross-wind directions. Taylor's hypothesis was observed to be valid for this case, by means of spatial correlation and temporal autocorrelation. The correlation drop matched well the correlation from observations. The correlations dropped to  
630 zero faster in the cell perturbation method cases, for both SOWFA and WRF-LES. Integration of the correlation curves yield the integral scales of the flow, shown in Fig. 4.

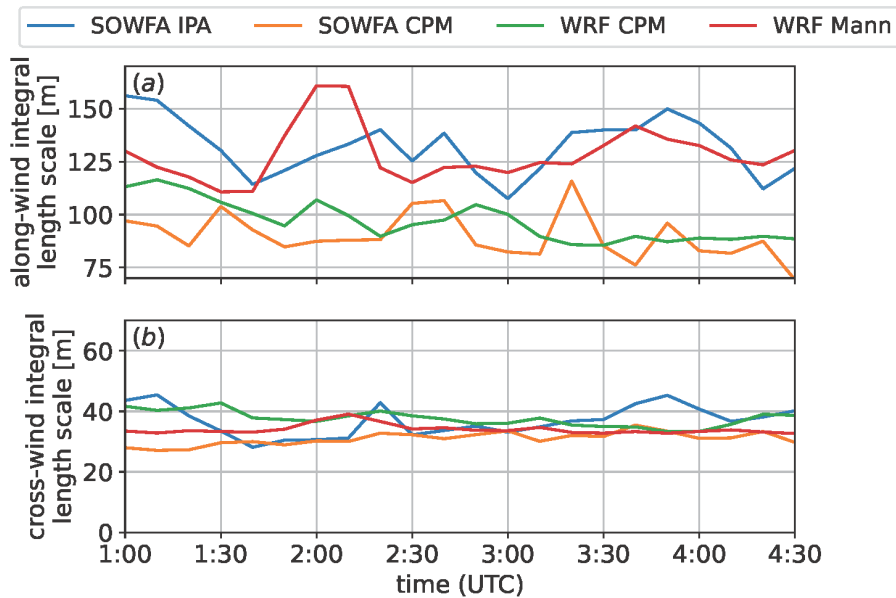


Figure 4: Integral length scales in the along-wind and cross-wind directions for each method.

635

The integral scales present in the cases that used the cell perturbation method to generate turbulence are smaller throughout the interval of interest. That is likely a result of the way the method works, by imposing small-scale disturbances in the temperature field, thus triggering high-frequency, small-scale turbulence that does little to change the integral scales of the flow as a whole. The Mann method, on the other hand, imposes large-scale turbulence, and the LES resolves the smaller scales. The larger scales imposed on the field are clearly observed when comparing the integral scales of the flow to those obtained using perturbation methods. Lastly, the SOWFA IPA case resulted in integral scale values comparable to the Mann method in WRF-LES. For this SOWFA approach, the turbulence is developed by the use of periodic boundary conditions, which allows (in both space and time) the development of large-scale structures, ultimately resulting in long correlation fetches, and thus, large integral length scale values. While the SOWFA IPA domain was overall smaller, it was nonetheless able to resolve scales of the order of 150 m as shown in Fig. 4. The integral scales in the cross-wind direction were of comparable magnitude in all cases investigated.

640

645

### 3.5.2 Alpha Ventus wind farm with generalized actuator disk – turbine comparison

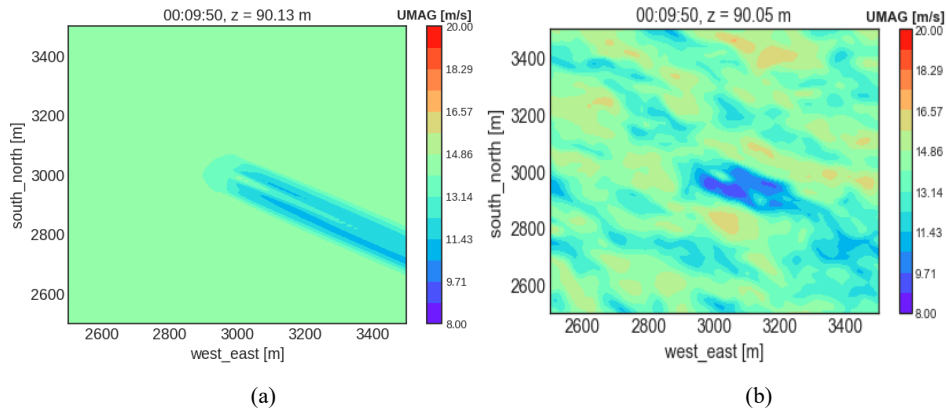
650

This section examines turbine wakes at the Alpha Ventus wind farm where the FINO1 tower is located. WRF to WRF-LES and WRF to SOWFA coupling approaches were extended to include a wind turbine parameterization using a GAD formulation (Mirocha et al., 2014a) as described in section 3.5. We refer to them as WRF-LES-GAD and WRF-SOWFA-GAD, and each compares using CPM at the inflow boundaries vs. not adding any turbulence.



655 The time window of interest is a 2-hour window starting at 0100 local time (0000 UTC) on 16 May 2010. We  
consider a single turbine (AV10) for the purpose of this study.

Figure 5 presents a qualitative visualization of turbine wakes in the horizontal plane at hub height for the WRF-LES-  
GAD approach. The LES domain is 6 km x 6 km, which provides a large fetch as well as downstream distance for  
660 wake propagation. However, only a region in the vicinity of the turbine is shown for clarity. As expected, the  
simulation without CPM does not resolve turbulence, and the resulting wake is what would be caused by an obstacle  
in the flow without any mixing. The simulation with CPM includes resolved turbulence, and hence mixing in the  
shear region, leading to a realistic wake. Figure 6 shows the flow field in the horizontal plane at hub height using the  
WRF-SOWFA-GAD approach with CPM. The entire domain is shown to demonstrate the fetch and the wake  
665 propagation region. We conclude that modeling realistic wakes requires using a turbulence generating method.



670 **Figure 5:** Wind speed at 01:10 local time on 16 May 2010 in the vicinity of the turbine (AV10) location using the WRF-LES-GAD approach for (a) no CPM and (b) CPM. A subset of the domain is shown.

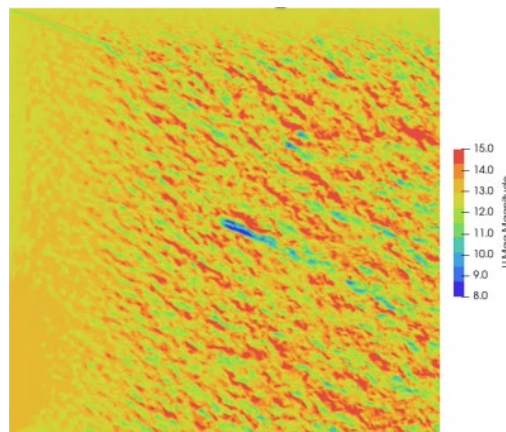


**Figure 6:** Wind speed at 01:10 local time on 16 May 2010 in the vicinity of the turbine (AV10) location using the WRF-SOWFA-GAD approach. The entire domain is shown.



### 675 3.6 Offshore Northeast U.S. coastal case

A second offshore case is archived that studies the impact of different ways of representing surface roughness and providing sea surface boundary conditions. The offshore environment in the Northeast United States is a hotbed for wind energy development. Observations have recorded occurrences of persistent low-level jets (LLJ) with jet noses commonly below hub height (Debnath et al., 2021). In this study we assess the sensitivity of LLJ characteristics (e.g., jet nose height, maximum wind speed, low-level shear, etc.) to SST. We utilize six freely available satellite-derived SST datasets from the Group for High Resolution SST website (Fig. 7) to vary the lower-boundary condition of surface temperature in online WRF simulations. The datasets used in this study are the Naval Oceanographic Office (NAVO; NASA, 2018) 1° dataset, Canadian Meteorological Center (CMC; Canada Meteorological Center, 2017) 1° SST product, the Office of Satellite and Product Operations (OSPO; OSPO, 2015) 0.54° dataset, the Operation Sea Surface Temperature and Sea Ice Analysis (OSTIA; UKMO, 2005) 0.54° dataset, the GOES-16 (NOAA, 2019) 0.02° SST product, and the Multiscale Ultrahigh Resolution (MUR; NASA, 2015) 0.01° product. The simulations consist of five domains with grid spacing spanning from 6,250 m to 10 m. We compare model results against observations from the New York State Energy Research and Development Authority floating lidars. We assess model performance in capturing the LLJ nose height, maximum wind speed, and low-level shear on each domain in order to compare how sensitive the results are to SST on the mesoscale and microscale. With this comparison, we aim to determine whether model sensitivity on the mesoscale translates directly to the microscale. In other words, can we expect the best performing mesoscale model setup to be the best setup on the microscale?

695

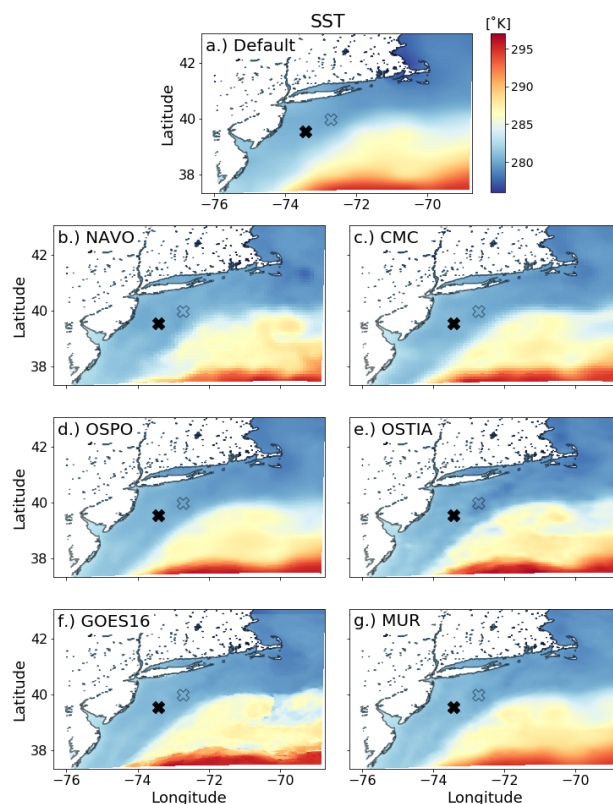
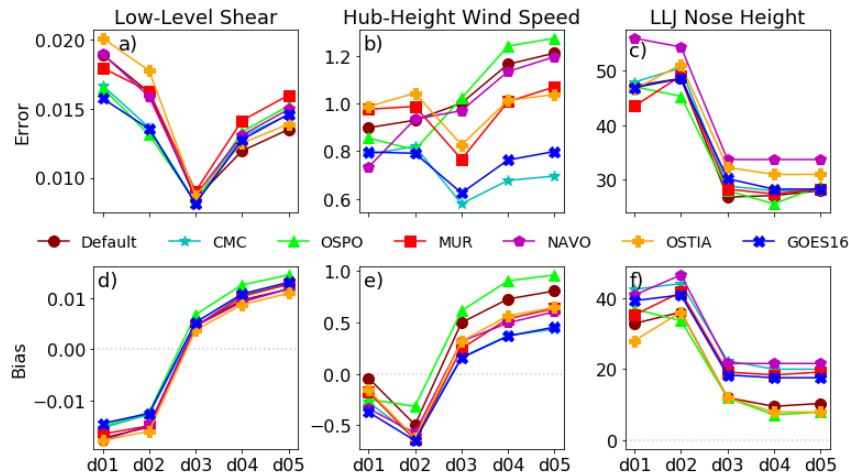


**Figure 7: Sea surface temperature datasets of varying resolution used as initial and surface boundary conditions over water.**

700 Results indicate that ensemble mean error and spread for various characteristics of the offshore LLJ vary between  
the mesoscale solutions and microscale solutions. However, variance within the microscale domains (domains 4 and  
5) is small. Error and bias of the low-level shear, hub-height wind speed (assumed to be 118 m in this case), and jet  
nose height (Fig. 8) vary across scales from mesoscale to microscale. Additionally, the best mesoscale performer did  
not lead to the best microscale performing setup in this case when considering these metrics. On the mesoscale, the  
705 shear produced in the lowest levels was lower than what was observed. The LES results improved upon the low-  
level shear but overcorrected the lowest level wind speeds and produced values lower than what were observed. It is  
suspected that using a drag force, locally consistent with MOST within the heterogeneous microscale simulation is  
the root cause of this overcorrection of low-level winds. Future work must focus on generalizing this finding in  
order to determine if mesoscale simulations can inform performance on the microscale prior to running simulations.



710

Figure 8: Error (top) and bias (bottom) for each case on each domain for low-level shear (left), hub-height wind speed (middle), and LLJ height (right).

#### 4 Contributions of enhanced methods

715

The MMC team additionally tested ways to improve the models both in terms of improved physics as well as to test the efficacy of machine learning methods.

#### 4.1 Three-dimensional planetary boundary layer

720

Traditional PBL schemes in mesoscale models are one-dimensional – that is, they parameterize only the vertical turbulent mixing under the assumption of horizontal homogeneity. In this sense, the vertical turbulent fluxes of momentum ( $\langle u'w' \rangle$  and  $\langle v'w' \rangle$ ), potential temperature ( $\langle \theta'w' \rangle$ ), water vapor mixing ratio ( $\langle q_v'w' \rangle$ ), and any other relevant scalars ( $\langle \phi'w' \rangle$ , where  $\phi$  is a scalar variable, such as cloud water mixing ratio) are computed. By definition, the horizontal homogeneity assumption neglects horizontal gradients in resolved quantities, as well as the vertical gradient in vertical velocity. Therefore, the vertical turbulent fluxes are dependent on only vertical gradients. However, this assumption is not justified at model resolutions in the *terra incognita* ( $\Delta \approx 100\text{--}1000$  m), where turbulence is partially resolved, and thus, horizontal gradients play an important role [e.g., Kosovic et al., 2021]. A main consequence of ignoring horizontal gradients in the *terra incognita* and under convective conditions is the development of spurious structures (termed modeled-convectively-induced secondary circulations, or M-CISCs, by Ching et al. (2004)], which can have a deleterious effect on the model solution. Furthermore, most 1D PBL parameterizations rely on the 2D horizontal diffusion scheme of Smagorinsky; however, this scheme was originally introduced for numerical stability and is therefore not physically motivated (Smagorinsky, 1990).

725

730

735

To address the fundamental research challenge of modeling in the *terra incognita*, our team has implemented the 3D PBL parameterization of Mellor and Yamada (Mellor, 1973; Mellor and Yamada, 1974; Mellor and Yamada, 1982) into the WRF model. This new parameterization does not impose the assumption of horizontal homogeneity;



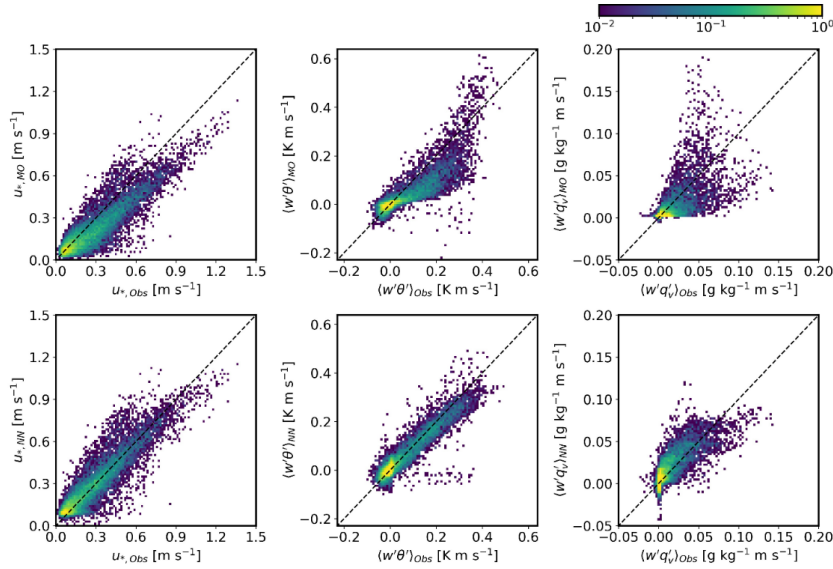
thus, it considers both vertical and horizontal gradients when computing all six momentum stresses and the full tensor for scalars (namely,  $\theta$  and  $q_v$ ), in addition to all components of the flux divergences. As a result, this approach does not require the use of Smagorinsky's 2D horizontal diffusion scheme and shows promise at grid resolutions in the *terra incognita*, especially under convective conditions. To examine the influence of accounting for horizontal gradients, we set up three different idealized model configurations under convective conditions and at high-resolution mesoscale grid spacing ( $\Delta = 250$  m): homogeneous surface forcing (rolls and cells), sea breeze front initiation, and mountain–valley circulation. Results clearly depict the suppression of M-CISCs by the 3D PBL scheme compared to a traditional 1D PBL scheme (Juliano et al., 2022). The impact of the turbulent length scale/closure constants formulation is found to be very important, such that M-CISCs may be present in the 3D PBL solution when the length scale is insufficiently large and thus vertical mixing is not strong enough.

#### 4.2 Machine learning surface layer scheme

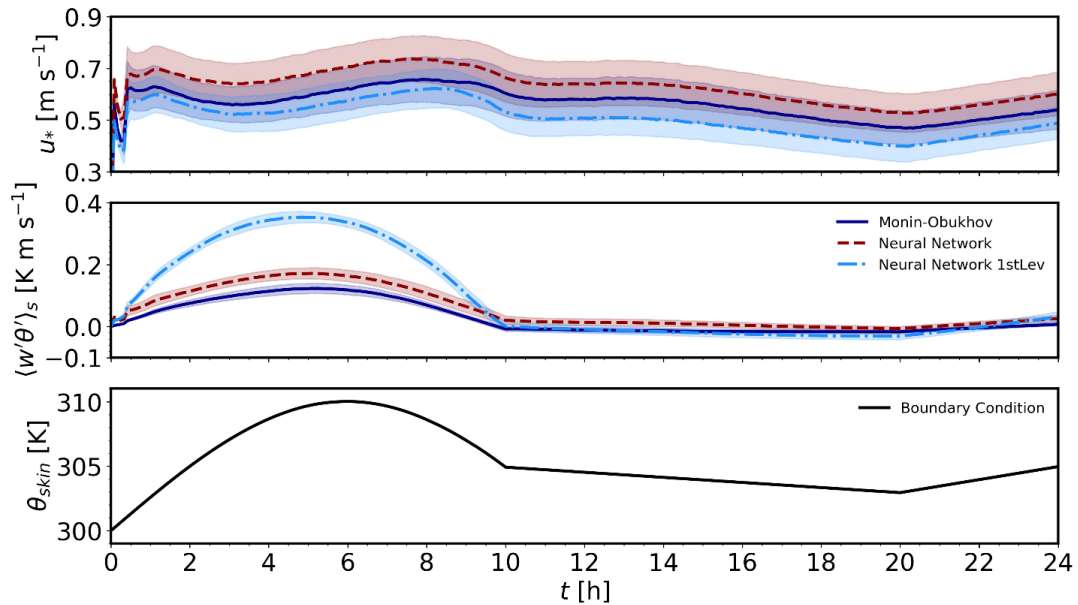
Specifying lower boundary conditions in numerical simulations of high-Reynolds-number atmospheric boundary flows requires estimating turbulent fluxes of momentum, heat, moisture, and other constituents. However, these fluxes are not known *a priori* and therefore must be parametrized. Parameterization of surface fluxes in atmospheric flow models at any scale, from global to turbulence-resolving large-eddy simulations, are based on MOST where atmospheric stability effects are accounted for through universal, semi-empirical stability functions. The stability functions are a function of the nondimensional stability parameter, a ratio of distance from the surface and the Obukhov length scale  $z/L$  (Monin and Obukhov, 1946). However, their functional form is determined based on observations using simple regression that cannot represent the surface-layer structure and governing parameters under a wide range of conditions. We have therefore developed and tested a neural network (NN) ML model for surface-layer parameterization (McCandless et al., 2022). We trained and tested the ML model using long-term observations from the National Oceanic and Atmospheric Administration's Field Research Division tower in Idaho and the Cabauw mast in the Netherlands. The comparison of MOST and the NN model surface-layer parameterizations with observations from the Cabauw mast are shown in Fig. 9. We then implemented the ML model in the FastEddy GPU-native LES model (Muñoz-Esparza et al., 2022) and the WRF model. The ML model implementation in Fast-Eddy demonstrates that it can accurately capture the diurnal evolution of an atmospheric boundary layer as shown in Fig. 10.

The ML model implementation in the WRF model was tested using a single-column model (SCM) based on the GABLS III intercomparison study case defined by Bosveld et al. (2014). The comparison of SCM simulations using the ML model surface-layer parameterization with observations and the MOST parameterization demonstrates that it can capture well the sensible heat flux, the skin temperature, the surface friction velocity, and the planetary boundary layer height, but underestimates the latent heat flux (Fig. 11).

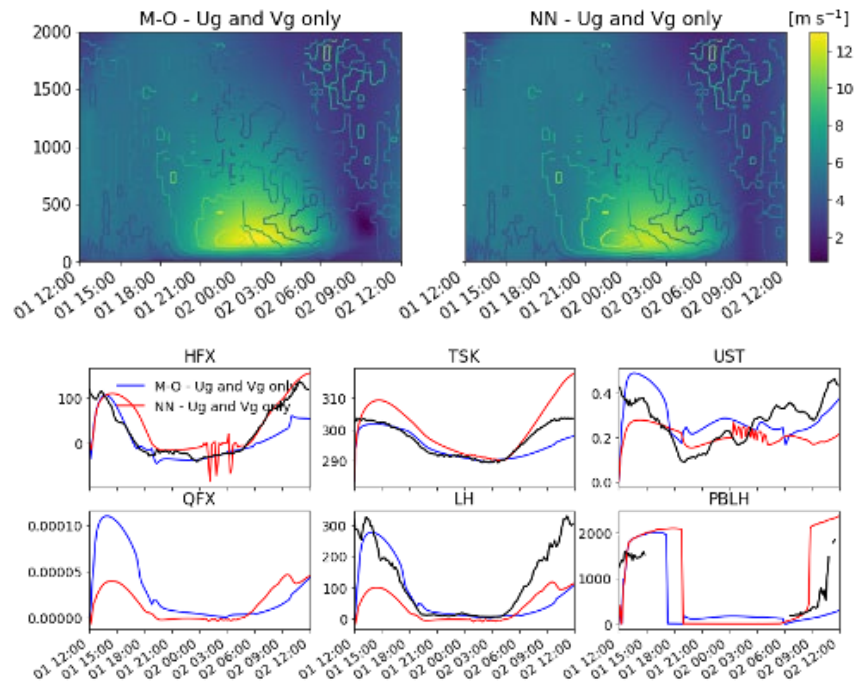




775 **Figure 9: Comparison of the MOST (top row) and an offline NN model (bottom row) surface-layer parameterizations of surface friction velocity (left panels), sensible heat flux (middle panels) and moisture flux (right panels) with observations from the Cabauw mast.**



780 **Figure 10: Comparison of the diurnal evolution of an ABL using the FastEddy LES model with the MOST and NN model surface-layer parameterizations: surface friction velocity (top panel), sensible heat flux (second panel), moisture flux (third panel), and surface skin temperature (bottom panel).**



785 **Figure 11: The SCM simulation of a GABLS III intercomparison study case using the WRF model.**

A potential reason for discrepancies between the ML model-predicted and observed latent heat flux is that the ML model for the surface-layer parameterization implemented in WRF interacts with a land-surface model, which is based on MOST.

790

The ML model for surface-layer parameterization demonstrates the potential to provide better estimates of surface fluxes in comparison to commonly used MOST-based parameterizations. However, to develop a generally applicable ML model it must be trained using long-term, consistent, complete, and quality-controlled observations from a wide range of environments. Future research could focus on expanding the training dataset and testing the model in mesoscale simulations over diverse locations.

795

### 4.3 Downscaling with deep learning

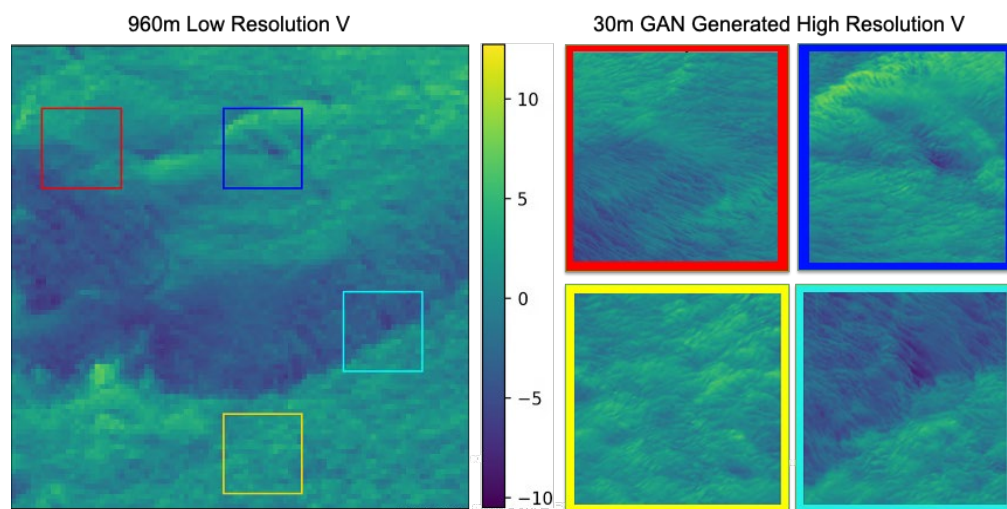
800 Microscale simulations, like the WRF-LES (30 m) generated over the Columbia River Basin for the Wind Forecast Improvement Project 2 (WFIP 2), are able to model the very complicated flow associated with complex terrain including downslope flows, mountain wakes, mountain-valley circulations, gravity waves, cold pools, and gap flows. However, such simulations are currently too complex to configure and computationally expensive for use outside the scientific research community. Here we tested using deep artificial neural networks on the LES to directly downscale from mesoscale to microscale in complex terrain. Once trained, deep learning models can



805 generate high-resolution simulations in just a few seconds from mesoscale input. In addition, we wished to  
demonstrate that the deep network models can then potentially be applied to regions other than the LES domain on  
which they were trained.

We created high-resolution/low-resolution training sample pairs by subtiling relevant vertical levels of the LES on  
810 the eastern portion of the domain and coarsening the tiles with average filters. We trained two separate Enhanced  
Super Resolution Generative Adversarial Networks (ESRGANs; Ledig et al., 2017; Wang et al., 2018) to  
accomplish the downscaling by training one GAN to downscale from 960 m to 240 m and the second GAN to  
downscale from 240 m to 30 m, and applying the models successively. We set aside data from every third time step  
in the LES for testing. Visually, the performance of the compound GAN architecture on testing data samples and the  
815 larger domain was impressive (Fig. 12). We performed statistical analysis of the high-resolution GAN generated  
wind and compared it with the LES, finding good agreement in the power spectra, velocity gradient distributions,  
and wind speed and wind direction distributions (Dettling et al., 2022). We found high Pearson correlation  
coefficients and very low mean bias between the tiles of GAN-generated wind components and LES, as well as good  
agreement in the moments of GAN-generated wind components with the LES, even in the higher-order moments,  
820 skewness, and kurtosis (Dettling et al., 2022).

To demonstrate the potential of transfer learning, we extended the testing sample set to include the western half of  
the WRF-LES, which contains part of Cascade Range including Mt. Hood. The western region is not only very  
unique when compared to the training region in the east, it is also topographically much more complex. We  
825 performed the same statistical analysis to compare the GAN-generated wind to the LES in the transfer learning  
region and the results were encouraging (Dettling et al., 2022).



830 **Figure 12:** Example of using the GAN to downscale from a coarsened 960 m resolution simulation (left image) to four  
example panels showing high-resolution 30 m generated images. The colors overlaid on the left panel correspond to the  
same color outlined image on the right panel.



## 5 Conclusions

We have summarized the results of the U.S. Department of Energy (DOE)-sponsored Mesoscale to Microscale  
835 Coupling (MMC) project that has focused on the best ways to couple the mesoscale to the microscale in order to  
better understand and model the transfer of energy from the largest scales of the atmosphere to those scales that  
directly affect harvesting that energy via wind turbines. The approach of using case studies based on observations  
has been a productive approach to test methodologies and has kept the findings grounded in real-world atmospheric  
behavior. The approach has required that we choose progressively more difficult cases, bringing in real-world  
840 complexity to better understand the implications of that complexity and how to best model it. We have studied how  
the mesoscale setup impacts the microscale results, applying consistent and appropriate boundary conditions,  
multiple methods of applying the coupling between scales, bridging the *terra incognita*, initializing turbulence at the  
microscale that is not resolved at the mesoscale, and applying these methods in complex terrain and in coastal and  
offshore environments. It is important to apply assessment metrics that are most appropriate for uses in wind energy,  
845 considering more than merely mean winds, but also sheer, veer, turbulence intensity, and turbulent kinetic energy  
via metrics such as energy spectra, pdfs along the flow, covariance, and proper orthogonal decomposition.

Some specific lessons learned include:

- 850 • Microscale simulations cannot necessarily improve matches to measurements if forced with an inaccurate  
mesoscale simulation (section 3.1).
- Idealized simulations may not well represent real-world phenomena and may be more difficult to initialize  
well than real cases.
- Microscale data assimilation (through profile assimilation on a periodic domain) requires an approach that  
855 allows the microscale to deviate from the mesoscale, otherwise wind and temperature profiles may not be  
in the correct equilibrium, resulting in unrealistic turbulence (Allaerts et al., 2020, 2022).
- High-quality potential temperature profiles, in addition to wind profiles, are necessary when performing  
microscale data assimilation with observational data (Allaerts et al., 2022; Jayaraman et al., 2022; Quon et  
al., 2022).
- Accurately capturing transitional atmospheric boundary layers and intermittent stable boundary layers  
860 remains a challenge (Allaerts et al., 2022; Quon et al., 2022).
- Without coupling across scales, even mesoscale flow is underresolved (Rai et al., 2019).
- Proper orthogonal decomposition analysis clearly indicates that the microscale contains energetic modes  
that originated from the mesoscale flow (Rai et al., 2019).
- The upper limit of the *terra incognita* is the boundary layer depth, indicating that horizontal spacing  
865 smaller than that (but larger than about 100 m) is likely to result in spurious secondary structures (Rai et al.,  
2019).



- Spurious roll features from the *terra incognita* can translate into unrealistic flow in the microscale (Rai, et al., 2019).
- 870 • Turbulence generation methods are necessary to avoid long fetches in developing turbulence at the microscale that is not resolved at the mesoscale (Section 2.4).
- Uncertainty can typically be traced to a small number of model parameters and the importance of these specific parameters can be interpreted in terms of flow physics considerations (Section 2.5).
- Certain conditions, such as complex terrain, can force gravity waves that reflect off of boundaries and grow to spurious amplitudes. Such gravity waves can be mitigated by Rayleigh damping (Section 2.6.2).
- 875 • The best mesoscale simulations don't always translate to the best match to wind-relevant metrics for the microscale simulation (Section 3.6).
- A three-dimensional planetary boundary layer can alleviate M-CISCS in the *terra incognita* (Section 4.1; Juliano et al., 2022).

880 Much research remains to be done to continue to enhance our understanding of the scales of atmospheric motion most relevant for harvesting wind energy. This team and the community have more work to do on the plethora of complex cases. More research is needed to further improve coupling technologies. For instance, more research is needed to understand why direct/indirect profile assimilation are successful in some cases and unsuccessful in others. We should also continue to explore topics of complexity, both on shore and off shore. Much remains to  
885 be learned through judiciously applying uncertainty quantification methods.

Although the current A2e MMC project has formally completed, we expect that its impact will live on, both in terms of providing code and methodologies that can be used by a wide range of wind farm modelers and in terms of being integrated into subsequent DOE wind energy projects. Specifically, DOE is initiating projects in offshore wind  
890 energy, complex terrain modeling for wind energy, and the impact of extreme events on modeling for wind energy.

In deploying renewable energy, we have become more cognizant of issues of fairness and justice to the people being impacted. In the United States, the Biden Administration's Justice40 Initiative (White House, 2022) seeks to deliver 40% of the overall benefits of climate investments to disadvantaged communities and inform equitable research,  
895 development, and deployment within the DOE, has recently highlighted the importance for energy justice considerations within the development of new energy systems. One of the major challenges of working in this space is finding actionable, effective paths forward while acknowledging and respecting the existing legacy of noninclusivity. Organizations such as the Initiative for Energy Justice and the Energy Equity Project (Initiative for Energy Justice, 2022) have established guidelines for working in the space of energy justice. Specifically these  
900 include: addressing the current perceptions that have been built on past practices; identifying uniquely disadvantaged people; procedural fairness; making sure that access is equally tenable; making sure the quality of service is equal across groups; and ensuring the desired impacts. Defined metrics can be used to determine whether or not a project is successful in working toward energy justice. While fairly centered on policymaking, these



905 assessment points can help guide the focus of renewable energy development, and act as a compass for what  
research objectives will have meaningful impact.

Finally, the MMC team wishes to thank all of the input from colleagues and community members throughout the  
course of this project. Our industry advisory panel and attendees to our various webinars and workshops have  
provided valuable input as to the directions that we have chosen and solutions that may be most practical for  
910 application to real-world needs. The biggest lesson learned is that it is through community cooperation that we are  
most likely to advance the science and technology needed to deploy the amounts of wind energy that the world will  
need for a carbon-free energy future.

915 **Author Contributions:** This paper results from a team effort to which all authors contributed. Project oversight and  
leadership plus management coordination was led by SEH with assistance from BK, LKB, CMK, JM, and MC. SD  
and MR provided oversight and resources from DOE, with MR providing overarching research goals and aims. EQ  
and PH led the software and data curation, with assistance from other authors. SEH led the preparation of the  
manuscript and all authors contributed.

920 **Competing Interests:** The authors declare that they have no conflict of interest.

925 **Acknowledgments:** This work was authored in part by the National Renewable Energy Laboratory, operated by  
Alliance for Sustainable Energy, LLC, for the U.S. Department of Energy (DOE) under Contract No. DE-AC36-  
08GO28308; Pacific Northwest National Laboratory (PNNL), operated by the Battelle Memorial Institute, for the  
U.S. DOE under Contract No. DE-A06-76RLO 1830; and Lawrence Livermore National Laboratory, operated by  
Lawrence Livermore National Security, for the U.S. DOE under Contract No. DE-AC52-07NA27344. Funding was  
provided by the U.S. Department of Energy Office of Energy Efficiency and Renewable Energy Wind Energy  
Technologies Office. The views expressed in the article do not necessarily represent the views of the DOE or the  
930 U.S. Government. The U.S. Government retains and the publisher, by accepting the article for publication,  
acknowledges that the U.S. Government retains a nonexclusive, paid-up, irrevocable, worldwide license to publish  
or reproduce the published form of this work, or allow others to do so, for U.S. Government purposes. The National  
Center for Atmospheric Research (NCAR) was a subcontractor to PNNL. NCAR is a major facility sponsored by the  
National Science Foundation under Cooperative Agreement No. 1852977.

935



## References

- 940 Adler, B., Wilczak, J. W., Bianco, L., Djalalova, I., Duncan Jr., J. B. and Turner, D.: Observational case study of a persistent cold pool and gap flow in the Columbia River basin. *J. Appl. Meteor. Climatol.*, 60, 1071–1090, <https://doi.org/10.1175/JAMC-D-21-0013.1>, 2021.
- 945 Allaerts, D., Quon, E., Draxl, C., and Churchfield, M.: Development of a Time-Height Profile Assimilation Technique for Large-Eddy Simulation. *Boundary-Layer Meteorology*, 176, 329–348. <https://doi.org/10.1007/s10546-020-00538-5>, 2020.
- Allaerts, D., Quon, E., and Churchfield, M.: Using observational mean-flow data to drive large-eddy simulations of a diurnal cycle at the SWIFT site. Submitted to *Wind Energy*, 2022.
- 950 Arthur, R. S., Mirocha, J. D., Marjanovic, N., Hirth, B. D., Schroeder, J. L., Wharton, S., and Chow, F.K.: Multi-scale simulation of wind farm performance during a frontal passage, *Atmosphere*, 11, 245, <https://doi.org/10.3390/atmos11030245>, 2020.
- 955 Arthur, R. S., Mirocha, J. D., Lundquist, K. A., and Street, R.L.: Using a canopy model framework to improve large-eddy simulations of the atmospheric boundary layer in the Weather Research and Forecasting model, *Mon.-Wea. Rev.*, 147(1), 31-52, <https://doi.org/10.1175/MWR-D-18-0204.1>, 2019.
- 960 Arthur, R. S., Juliano, T. W., Adler, B., Krishnamurthy, R., Lundquist, J. K., Kosović, B., and Jiménez, P. A.: Improved representation of horizontal variability and turbulence in mesoscale simulations of an extended cold-air pool event. *Journal of Applied Meteorology and Climatology*, 61(6), 685–707, <https://doi.org/10.1175/JAMC-D-21-0138.1>, 2022.
- 965 Berg, L. K., Liu, Y., Yang, B., Qian, Y., Olson, J., Ma, P.-L., and Hou, Z.: Sensitivity of turbine-height wind speeds to parameters in the planetary boundary-layer parametrization used in the Weather Research and Forecasting model: Extension to wintertime conditions. *Boundary-Layer Meteorology*, 170, 507-518. <http://dx.doi.org/10.1007/s10546-018-0406-y>, 2019.
- Berkooz, G., Holmes, P., and Lumley, J.L.: The proper orthogonal decomposition in the analysis of turbulent flows, *Annu. Rev. Fluid Mech.*, 25, 539-75, <https://doi.org/10.1146/annurev.fl.25.010193.002543>, 1993.
- 970 Bosveld, F. C., Baas, P., van Meijgaard, E., de Bruijn, E. I. F., Steeneveld, G.-J., and Holtslag, A. A. M.: The Third GABLS Intercomparison Case for Evaluation Studies of Boundary-Layer Models. Part A: Case Selection and Set-Up. *Boundary-Layer Meteorology*, 152, 133–156. <https://doi.org/10.1007/s10546-014-9919-1>, 2014.
- 975 Bou-Zeid, E., Meneveau, C. and Parlange, M. B.: A scale-dependent Lagrangian dynamic model for large eddy simulation of complex turbulent flows. *Phys. Fluids*, 17, 025105, <https://doi.org/10.1063/1.1839152>, 2005.
- Brasseur, J. G., and T. Wie, T: Designing large-eddy simulation of the turbulent boundary layer to capture law-of-the-wall scaling, *Phys. Fluids*, 22, 021303, <https://doi.org/10.1063/1.3319073>, 2010.
- 980 Brown, A. R., Hobson, J. M. and Wood, N.: Large-eddy simulation of neutral turbulent flow over rough sinusoidal ridges, *Bound.-layer Meteorol.*, 98, 411–441. DOI:10.1023/A:1018703209408, 2001.
- 985 Canada Meteorological Center. GHRSSST Level 4 CMC0.1deg Global Foundation Sea Surface Temperature Analysis (GDS version 2), <https://doi.org/10.5067/GHCMC-4FM03>, 2017.
- Ching, J., Rotunno, R., LeMone, M., Martilli, A., Kosović, B., Jiménez, P. A., and Dudhia, J.: Convectively induced secondary circulations in fine-grid mesoscale numerical weather prediction models. *Mon. Wea. Rev.*, 142, 3284–3302, <https://doi.org/10.1175/MWR-D-13-00318.1>, 2014.



- 990 Chow, F. K., Street, R. L., Xue, M. and Ferziger, J.H.: Explicit filtering and reconstruction turbulence modeling for large-eddy simulation of neutral boundary layer flow, *J. Atmos. Sci.*, 62, 2058–2077, <https://doi.org/10.1175/JAS3456.1>, 2004.
- 995 Debnath, M., Doubrawa, P., Optis, M., Hawbecker, P., and Bodini, N.: Extreme wind shear events in US offshore wind energy areas and the role of induced stratification. *Wind Energy Science*, 6(4), 1043-1059. <https://doi.org/10.5194/wes-6-1043-2021>, 2021.
- 1000 Dettling, S., Brummet, T., Gagne, D.J., Kosovic, B., and Haupt, S.E.: Downscaling from Mesoscale to Microscale in Complex Terrain using a Generative Adversarial Network, to be submitted to *Artificial Intelligence for the Environmental Sciences*, 2022.
- 1005 Draxl, C., Allaerts, D., Quon, E., and Churchfield, M.: Coupling Mesoscale Budget Components to Large-Eddy Simulations for Wind-Energy Applications. *Boundary-Layer Meteorology*, 179, 73-98. <https://doi.org/10.1007/s10546-020-00584-z>, 2021.
- 1010 Eghdami, M., Barros, A. P., Jiménez, P. A., Juliano, T. W., and Kosovic, B.: Diagnosis of Second-Order Turbulent Properties of the Surface Layer for Three-Dimensional Flow Based on the Mellor–Yamada Model. *Monthly Weather Review*, 150(5), 1003-1021. <https://doi.org/10.1175/MWR-D-21-0101.1>, 2022.
- 1010 Gopalan, H., Gundling, C., Brown, K., Roget, B., Sitaraman, J., Mirocha, J.D., and Miller, W. O.: A Coupled Mesoscale-Microscale Framework for Wind Resource Estimation and Farm Aerodynamics, *J. Wind Eng. Ind. Aerodyn.* **132**, 13–26, [10.1016/j.jweia.2014.06.001](https://doi.org/10.1016/j.jweia.2014.06.001), 2014.
- 1015 Haupt, S.E., Kosovic, B., Shaw, W., Berg, L., Churchfield, M., et al.: On Bridging a Modeling Scale Gap: Mesoscale to Microscale Coupling for Wind Energy, *Bulletin of the American Meteorological Society*, Dec. 2019, 2533-2549, <https://journals.ametsoc.org/doi/full/10.1175/BAMS-D-18-003>, 2019.
- 1020 Haupt, S.E., Allaerts, D., Berg, L., Churchfield, M., DeCastro, A., Draxl, C., Gagne, D.J., Hawbecker, P., Jimenez, P., Jonko, A., Juliano, T., Kaul, C., Kosovic, B., McCandless, T., Mirocha, J., Munoz-Esparza, D., Quon, E., Rai, R., Sauer, J., Shaw, W.: FY19 Report of the Atmosphere to Electrons Mesoscale to Microscale Coupling Project: Pacific Northwest Laboratory Report PNNL-29603, 127 pp. <https://doi.org/10.2172/1735568>, 2019.
- 1025 Haupt, S.E., Arthur, R., Berg, L., Churchfield, M., DeCastro, A., Dettling, S., Draxl, C., Gagne, D.J., Hawbecker, P., Jimenez, P., Jonko, A., Juliano, T., Kaul, C., Kosovic, B., Lassman, Kumar, M., W. McCandless, T.C., Mirocha, J., Quon, E., Rai, R., Shaw, W., Thedin, R.: FY20 Report of the Atmosphere to Electrons Land-Based Mesoscale to Microscale Coupling Project: Pacific Northwest Laboratory Report PNNL-30841, 104 pp. 2020
- 1030 Hawbecker, P., & Churchfield, M.: Evaluating Terrain as a Turbulence Generation Method. *Energies*, 14(21), 6858, <https://doi.org/10.3390/en14216858>, 2021.
- 1035 Hawbecker, P.; Lassman, W.; Juliano, T. W.; Kosovic, B., Haupt S.E.: Model sensitivity across scales. To be submitted to *Atmosphere*, 2022.
- 1035 Hirth, B., Schroeder, J.: A summary of the National Wind Institute meteorological measurement facilities at the Texas Tech University’s Reese Technology Center field site. Texas Tech University, Lubbock, TX. 2014.
- Initiative for Energy Justice, <https://iejusa.org/>, last access: 30 November 2022.
- 1040 Jayaraman, B., Quon, E., Li, J., and Chatterjee, T.: Structure of offshore low-level jet turbulence and implications to mesoscale-to-microscale coupling, *Journal of Physics: Conference Series*, The Science of Making Torque from Wind (TORQUE 2022), **2265** 022064, doi:10.1088/1742-6596/2265/2/022, 2022.
- 1045 Jiménez, P. A., & Dudhia, J.: On the need to modify the sea surface roughness formulation over shallow waters. *Journal of Applied Meteorology and Climatology*, 57(5), 1101-1110. 2018.





- Jonkman, B. J., : TurbSim user's guide. No. NREL/TP-500-39797. National Renewable Energy Lab.(NREL), Golden, CO (United States), 2006.
- 1050 Juliano, T. W., Kosović, B., Jiménez, P. A., Eghdami, M., Haupt, S. E., and Martilli, A.: Gray zone” simulations using a three-dimensional planetary boundary layer parameterization in the Weather Research and Forecasting model, *Monthly Weather Review*, 150, 1585–1619. DOI: <https://doi.org/10.1175/MWR-D-21-0164.1>, 2022.
- 1055 Kaul, C. M., Hou, Z. J., Zhou, H., Rai, R. K., & Berg, L. K.: Sensitivity analysis of wind and turbulence predictions with mesoscale-coupled large eddy simulations using ensemble machine learning. *Journal of Geophysical Research: Atmospheres*, 127, e2022JD037150. <https://doi.org/10.1029/2022JD037150>, 2022.
- Kelley, C.L., Ennis, B.L.: SWIFT site atmospheric characterization (No. SAND2016- 0216). Sandia National Laboratories, Albuquerque, NM. <https://doi.org/10.2172/1237403>, 2016.
- 1060 Khani, S., and Porté-Agel, F.: A modulated-gradient parametrization for the large eddy simulation of the atmospheric boundary layer using the Weather Research and Forecasting model, *Bound.-Layer Meteorol.*, **165**(3), 385–404, 2017.
- 1065 Kirkil, G., Mirocha, J. D., Bou-Zeid, E., Chow, F. K. and Kosović, B.: Implementation and Evaluation of Dynamic Subfilter-Scale Stress Models for Large-Eddy Simulation using WRF, *Mon. Wea. Rev.*, 140, 266-284. <http://dx.doi.org/10.1175/MWR-D-11-00037.1>, 2012.
- 1070 Kosović, B., Munoz, P. J., Juliano, T. W., Martilli, A., Eghdami, M., Barros, A. P., & Haupt, S. E.: Three-dimensional planetary boundary layer parameterization for high-resolution mesoscale simulations. In *Journal of Physics: Conference Series* (Vol. 1452, No. 1, p. 012080). IOP Publishing. 2020.
- 1075 Kosović, B., Jimenez, P. A., Juliano, T. W., Eghdami, M., & Haupt, S. E.: Analysis of Horizontal Shear and Mixing at Gray Zone Length Scales Using Filtered Large-Eddy Simulation of a Flow over Complex Terrain. In 101st American Meteorological Society Annual Meeting. AMS., 2021, January.
- Ledig, C., Theis, L., Huszar, F., Caballero, J., Cunningham, A., Acosta, A., Aitken, A., Tejani, A., Totz, J., Wang, Z., and Shi, W. : Photo-Realistic Single Image Super-Resolution Using a Generative Adversarial Network, <https://arxiv.org/abs/1609.04802>, 2017.
- 1080 Liu, Y., Warner, T., Vincent, C. L., Wu, W., Mahoney, W., Swerdlin, S., Parks, K., and Boehmert, J.: Simultaneous nested modeling from the synoptic scale to the LES scale for wind energy applications, *J. Wind Eng. Ind. Aerodyn.* 99(4), 308–319, 2011.
- 1085 Mann, J.: Wind field simulation. *Probabilistic engineering mechanics* 13.4 (1998): 269-282, 1998.
- Mason, P. J., and Thomson, D. J.: Stochastic backscatter in large-eddy simulations of boundary layers, *J. Fluid Mech.*, **242**, 51-78, 1992.
- 1090 Mazzaro, L.J., Koo, E., Muñoz-Esparza, D., Lundquist, J. K. and Linn, R. R.: Random Force Perturbations: A New Extension of the Cell Perturbation Method for Turbulence Generation in Multiscale Atmospheric Boundary Layer Simulations. *J. Advances in Modeling Earth Systems*, 11, 2311–2329, doi:10.1029/2019MS001608, 2019.
- 1095 McCandless, T., Gagne, D. J., Kosović, B., Haupt, S. E., Yang, B., Becker, C., and Schreck, J.: Machine Learning for Improving Surface-Layer-Flux Estimates. *Boundary-Layer Meteorology*, <https://doi.org/10.1007/s10546-022-00727-4>, 2022.
- Mellor, G. L.: Analytic prediction of the properties of stratified planetary surface layers. *J. Atmos. Sci.*, 30, 1061–1069, 1973.
- 1100 Mellor, G. L., and Yamada, T.: A hierarchy of turbulence closure models for planetary boundary layers. *J. Atmos. Sci.*, 31, 1791–1806, 1974.



- 1105 Mellor, G. L., and Yamada, T.: Development of a turbulence closure model for geophysical fluid problems. *Rev. Geophys.*, 20, 851–875, 1982.
- Mirocha, J. D., Kosović, B., Aitken, M. L., and Lundquist, J. K.: Implementation of a generalized actuator disk wind turbine model into the weather research and forecasting model for large-eddy simulation applications, *J. Renew. Sustain. Energy*, 6, <http://dx.doi.org/10.1063/1.4861061>, 2014a.
- 1110 Mirocha, J. D., Kosović, B. and Kirkil, G.: Resolved turbulence characteristics in large-eddy simulations nested within mesoscale simulations using the Weather Research and Forecasting model, *Mon. Wea. Rev.*, 142, 806–831. <http://dx.doi.org/10.1175/MWR-D-13-00064.1>, 2014b.
- 1115 Mirocha, J. D., Kirkil, G., Bou-Zeid, E., Chow, F. K., and Kosović, B.: Transition and equilibration of neutral atmospheric boundary layer flow in one-way nested large-eddy simulations using the Weather Research and Forecasting model, *Mon. Wea. Rev.*, 141, 918–940. <http://dx.doi.org/10.1175/MWR-D-11-00263.1>, 2013.
- Mirocha, J. D., Lundquist, J. K., and Kosović, B.: Implementation of a nonlinear subfilter turbulence stress model for large-eddy simulation in the Advanced Research WRF Model, *Mon. Wea. Rev.*, 138, 4212–4228. <http://dx.doi.org/10.1175/2010MWR3286.1>, 2010.
- 1120 Monin, A. S., and Obukhov, A. M. F.: Basic laws of turbulent mixing in the surface layer of the atmosphere. *Tr. Geofiz. Inst., Akad. Nauk SSSR*, 24, 163–187, 1954.
- 1125 Muñoz-Esparza, D. and Kosovic, B.: Generation of inflow turbulence in large-eddy simulations of nonneutral atmospheric boundary layers with the cell perturbation method. *Mon. Wea. Rev.*, 146:1889–1909. doi:10.1175/MWR-D-18-0077.1, 2018.
- 1130 Muñoz-Esparza, D., Kosović, B., van Beek, J. and Mirocha, J. D.: A stochastic perturbation method to generate inflow turbulence in large-eddy simulation models: application to neutrally stratified atmospheric boundary layers, *Phys. Fluids*, 27, 035102, <http://dx.doi.org/10.1063/1.4913572>, 2015.
- Muñoz-Esparza, D., Kosović, B., Mirocha, J. D. and van Beek, J.: Bridging the transition from mesoscales to microscale turbulence in atmospheric models, *Bound.-Layer Meteorol.*, 153(3), 409–440, <http://dx.doi.org/10.1007/s10546-014-9956-9>, 2014.
- 1135 Muñoz-Esparza, D., Becker, C., J Sauer, . A., Gagne II, D. J., Schreck, J. and Kosović, B.: On the application of an observations-based machine learning parameterization of surface layer fluxes within an atmospheric large-eddy simulation model. *Journal Geophysical Research*, 127, <https://doi.org/10.1029/2021jd036214>, 2022.
- 1140 Nakanishi, M. and Niino, H: An improved mellor–yamada level 3 model: its numerical stability and application to a regional prediction of advecting fog. *Bound.-Layer Meteor.*, 119, 397–407, 2006.
- 1145 NASA Jet Propulsion Laboratory. GHRSSST Level 4 MUR Global Foundation Sea Surface Temperature Analysis (v4.1), <https://doi.org/10.5067/GHGMR-4FJ04>, 2015.
- NASA Jet Propulsion Laboratory. GHRSSST Level 4 K10\_SST Global 10 km Analyzed Sea Surface Temperature from Naval Oceanographic Office (NAVO) in GDS2.0, <https://doi.org/10.5067/GHK10-L4N01>, 2018.
- 1150 NOAA/NESDIS/STAR. GHRSSST NOAA/STAR GOES-16 ABI L3C America Region SST. Ver. 2.70, <https://doi.org/10.5067/GHG16-3UO27>, 2019.
- OpenFAST, GitHub repository, <https://github.com/OpenFAST/openfast>, 2022.
- 1155 OSPO. GHRSSST Level 4 OSPO Global Foundation Sea Surface Temperature Analysis (GDS version 2), <https://doi.org/10.5067/GHG16-3UO27>, 2015.



- 1160 Patton, E. G., and Finnigan, J. J.: Canopy turbulence. Handbook of environmental fluid 706 dynamics, H. J. S. Fernando, Ed., Vol. 1, CRC Press, chap. 24, 311–328, 2012.
- Quon, E. W.: Measurement-Driven Large-Eddy Simulations of a Wind Turbine Array during a Wake Steering Field Campaign. Under submission to *Wind Energy Science*, 2022.
- 1165 Rai, R.K., Berg, L.K., Kosovic, B., Mirocha, J. D., Pekour, M. S., and Shaw, W. J.: Comparison of measured and numerically simulated turbulence statistics in a convective boundary layer over complex terrain. *Boundary-Layer Meteorology*, 163, 69–98, 2017.
- 1170 Rai, R.K., Berg, L. K., Kosovic, B., S.E. Haupt, S. E., Mirocha, J. D., Ennis, B., and Draxl, C.: Evaluation of the Impact of Horizontal Grid Spacing in Terra Incognita on Coupled Mesoscale-microscale Simulations using the WRF Framework. *Monthly Weather Review*, 147, 1007– 1027. <https://journals.ametsoc.org/doi/abs/10.1175/MWR-D-18-0282.1>, 2019.
- 1175 Rinker, J.M.: PyConTurb: an open-source constrained turbulence generator, *Journal of Physics: Conference Series*, 1037(6), 1037 06032. DOI 10.1088/1742-6596/1037/6/062032. 2018.
- Rybchuk, A., Juliano, T. W., Lundquist, J. K., Rosencrans, D., Bodini, N., and Optis, M.: The Sensitivity of the Fitch Wind Farm Parameterization to a Three-Dimensional Planetary Boundary Layer Scheme, *Wind Energy. Sci. Discuss.* [preprint], <https://doi.org/10.5194/wes-2021-127>, accepted for publication, 2022.
- 1180 Shaw, W.J., Berg, L.K., Cline, J., Draxl, C., Djalalova, E., et al.: The second wind forecasting improvement project (WFIPs): General overview, *Bull. American Meteorol. Soc.*, 100(9), 1687–1699, <https://doi.org/10.1175/BAMS-D-18-0036.1>, 2021
- 1185 Shaw, R. H., and Patton, E. G.: Canopy element influences on resolved-and subgrid-scale 716 energy within a large-eddy simulation. *Agr. For. Meteorol.*, 115, 5–17, 2003.
- 1190 Skamarock, W. C., Klemp, J. B., Dudhia, J., Gill, D. O., Barker, D., Duda, M. G., ... Powers, J. G.: A Description of the Advanced Research WRF Version 3 (No. NCAR/TN-475+STR). University Corporation for Atmospheric Research. doi:10.5065/D68S4MVH, 2008.
- Smagorinsky, J.: General circulation experiments with the primitive equations, I. The basic experiment, *Mon. Wea. Rev.*, 91(3), 99–164, [https://doi.org/10.1175/1520-0493\(1963\)091<0099:GCEWTP>2.3.CO;2](https://doi.org/10.1175/1520-0493(1963)091<0099:GCEWTP>2.3.CO;2), 1963.
- 1195 Smagorinsky J.,: Some Historical Remarks on the Use of Non-linear Viscosities in Geophysical Models. *Proc Int Workshop Large Eddy Simul We Stand Eds.*, 1-3, 1990 Dec 19.
- 1200 Thedin, R., Quon, E., Churchfield, M., and Veers, E.: Investigations of Correlation and Coherence in Turbulence from a Large-Eddy Simulation, *Wind Energ. Sci. Discuss.* [preprint] in review, <https://doi.org/10.5194/wes-2022-71>, 2022.
- Thedin, R., Lassman, W, Rai, R.K., Hawbecker, P., Nikolic, J. Churchfield, M., Mirocha, J.D., Kaul, C. and Haupt, S.E.: A comparison of Mesoscale-to-microscale coupling approaches applied to an offshore environment, to be submitted to *Wind Energy Science*, 2022.
- 1205 UKMO. GHRSSST Level 4 OSTIA Global Foundation Sea Surface Temperature Analysis: <https://doi.org/10.5067/GHOST-4FK01>, 2005.
- 1210 Wang, X., Yu, K., Wu, S., Gu, J., Liu, Y., Dong, C., Loy, C.C., Qian, Y., and Tang, X.: ESRGAN: Enhanced Super-Resolution Generative Adversarial Networks, *Computer Vision and Pattern Recognition*, <https://arxiv.org/abs/1809.00219v2>, 2018.
- White House, Justice40, a Whole of Government Initiative, <https://www.whitehouse.gov/environmentaljustice/justice40/>, last access: 30 November 2022.



- 1215 Wilczak, J. M., Stoelinga, M., Berg, L. K., Sharp, J., Draxl, C., McCaffrey, K., Banta, R. M., Bianco, L., Djalalova, I., Lundquist, J. K., and Muradyan, P.: The second wind forecast improvement project (WFIP2): Observational field campaign. *Bulletin of the American Meteorological Society*, 100(9):1701-23., 2019.
- 1220 Wyngaard, J. C., 2004: Toward Numerical Modeling in the “Terra Incognita.” *J. Atmos. Sci.* 61, 1816–1826.
- 1225 Yang, B., Berg, L. K., Qian, Y., Wang, C., Hou, Z., Liu, Y., et al.: Parametric and structural sensitivities of turbine-height wind speeds in the boundary layer parameterizations in the Weather Research and Forecasting model. *Journal of Geophysical Research: Atmospheres*, 124 , 5951-5969. doi: 10.1029/2018JD029691, 2019.
- Yang, B., Qian, Y., Berg, L. K., Ma, P.-L., Wharton, S., Bulaevskaya, V., et al.: Sensitivity of turbine-height wind speeds to parameters in planetary boundary-layer and surface-layer schemes in the Weather Research and Forecasting model. *Boundary-Layer Meteorology*, 162 , 117-142, 2017.
- 1230 Zajaczkowski, F. J., Haupt, S.E. and Schmehl, K.J.: A Preliminary Study of Assimilating Numerical Weather Prediction Data into Computational Fluid Dynamics Models for Wind Prediction, *J. Wind Eng. Ind. Aerodyn.* **99**, 320–329 doi:10.1016/j.jweia.2011.01.023, 2011.
- 1235 Zuidema, P., Chang, P., Medeiros, B., Kirtman, B. P., Mechoso, R., Schneider, E. K., ... & Xu, Z.: Challenges and prospects for reducing coupled climate model SST biases in the eastern tropical Atlantic and Pacific oceans: The US CLIVAR Eastern Tropical Oceans Synthesis Working Group. *Bulletin of the American Meteorological Society*, 97(12), 2305-2328, 2016.